

Review article



Live-cell imaging powered by computation

Hari Shroff¹, Ilaria Testa¹ , Florian Jug¹ , Suliana Manley¹

Abstract

The proliferation of microscopy methods for live-cell imaging offers many new possibilities for users but can also be challenging to navigate. The prevailing challenge in live-cell fluorescence microscopy is capturing intra-cellular dynamics while preserving cell viability. Computational methods can help to address this challenge and are now shifting the boundaries of what is possible to capture in living systems. In this Review, we discuss these computational methods focusing on artificial intelligence-based approaches that can be layered on top of commonly used existing microscopies as well as hybrid methods that integrate computation and microscope hardware. We specifically discuss how computational approaches can improve the signal-to-noise ratio, spatial resolution, temporal resolution and multi-colour capacity of live-cell imaging.

Sections

Introduction

Improving the SNR

Improving spatial resolution

Improving temporal resolution

Multi-colour imaging

Discussion and outlook

¹Janelia Research Campus, Howard Hughes Medical Institute (HHMI), Ashburn, VA, USA. ²Department of Applied Physics and Science for Life Laboratory, KTH Royal Institute of Technology, Stockholm, Sweden. ³Fondazione Human Technopole (HT), Milan, Italy. ⁴Institute of Physics, School of Basic Sciences, Swiss Federal Institute of Technology Lausanne (EPFL), Lausanne, Switzerland. e-mail: suliana.manley@epfl.ch

Introduction

An essential feature of living systems is that they are dynamic. Molecules form complexes at specific locations and times, initiating and propagating cascades of reactions. Organelles change size, shape, composition and organization within the cell, exchanging signals and molecules as they contact each other. Cells migrate, divide and differentiate to specialize within a tissue. Thus, sequences of events encode causal relationships and reveal mechanistic details, from the molecular to organismal scale. Fluorescence microscopy, which enables dynamic imaging of specific molecules, their interactions and biochemical states in living samples, is thus an important tool for biological discovery. Yet, interpreting image data requires quantitative analysis – this is where computation, through automated image-processing pipelines, typically takes over. Such analyses have yielded insights into modes and rates of motion, through image segmentation and object tracking^{1–4}, or molecular exchange and binding kinetics, through photobleaching recovery, photo-activation and single-particle tracking^{5–8}. However, advances in computational approaches, particularly through deep learning^{9–11} (Box 1), also have important implications for experimental design, and are shifting the boundaries of what is possible to capture in living systems. To better understand the potential of computation in live-cell imaging, it is useful to consider current limitations to live microscopic acquisitions.

The ideal microscopy measurement of a living specimen captures dynamics with molecular specificity, at relevant structural scales, without introducing perturbations. What does this mean practically, in terms of image quality? The signal-to-noise ratio (SNR) should be high enough to enable quantitative analysis; the spatial resolution should be high enough to distinguish functional molecular organization; the temporal resolution should be high enough to capture dynamic intermediate states; and enough channels, to image fluorophores of different colours or lifetimes, should be collected in parallel to reveal molecular interaction partners. Additional requirements based on the biological system further constrain the measurement. Different measurement aspects, although independently determined by microscope hardware, are entangled due to their common dependence on the amount of fluorescence emitted by the sample (the photon budget). We refer to photon budget both because fluorescent molecules can only emit a limited number of photons before irreversibly photobleaching, and because living samples can endure exposure to limited irradiance before suffering from photodamage. The resulting tradeoffs between these measurement properties lead to the ‘pyramid of frustration’, where an improvement along one dimension requires a sacrifice along others, within a given imaging framework¹². As an example, acquiring images with less light can prolong imaging experiments but also results in noisy or lower-resolution data.

Computational approaches can work synergistically with other developments to expand the possible accessible measurement properties as defined by the photon budget. Other technological advances include developing fluorophores with higher photostability to increase the number of photons per molecule^{13–15}, harnessing fluorophore transitions between photophysical states to enable super-resolution microscopy^{16–19} and shaping the excitation beam, as in light-sheet microscopy and multiphoton microscopy^{20,21}, to reduce out-of-focus exposure and phototoxicity. Unlike these approaches, computation further extends the range of biological phenomena that can be captured using microscopy without having to change the sample or the microscope hardware.

Here, we provide an overview of recent developments in the field of computational microscopy, focusing on those that boost aspects

important for live fluorescence imaging: SNR, spatial resolution, temporal resolution and multi-colour acquisition. We review computational tools that can be easily combined with existing microscopies or used to create hybrid methods that integrate computation and microscope hardware (Fig. 1a). We define technical terms and summarize the methods reviewed as well as their advantages, requirements, potential artefacts, how they were demonstrated, and links to their software (Table 1). Throughout, we distinguish between tools that are at ready-to-use versus proof-of-concept stage and suggest new opportunities ripe for exploration.

Improving the SNR

Signal and noise are fundamentally tied to image quality. In the context of fluorescence microscopy, signal is related to the amount of fluorescence emitted by the sample and captured by the detector. Not all fluorescence is desirable: so-called ‘background’ fluorescence can arise due to non-specific staining, out-of-focus planes, scattering or sample autofluorescence. Additionally, since fluorescence emission is a stochastic process, signal intensity fluctuates over time, introducing noise. Imaging systems introduce additional noise, such as detector ‘read noise’ arising from analogue-to-digital conversion, and ‘dark current’ or thermal noise that is present even in the absence of fluorescence. As a fundamental property of the signal and its detection, noise exists even in the absence of background fluorescence. The relevant parameter is the relative proportion of signal and noise – or the SNR – since it determines the useful information that can be extracted from images.

SNR has important implications for live fluorescence imaging: in most experiments, the photon budget is limiting. During imaging, fluorophores bleach, thereby lowering the SNR. When the SNR approaches 1, a useful signal can no longer be discerned from noise and the experiment is effectively over. While a higher SNR is always desirable, for live imaging, sample health must also be preserved¹². Given that a higher SNR can be achieved through increased excitation dose, which increases the production rate of damaging reactive oxygen species, the tradeoff between the SNR and phototoxicity is salient. Additionally, methods that afford higher spatial resolution generally deplete fluorescence more rapidly than alternatives, implying a tradeoff between the SNR and spatial resolution. Finally, because noise is intrinsic to the imaging process, no two fluorescence images of the same sample are identical. Thus, any fluorescence image is, at best, an estimate of the underlying sample and the SNR limits data interpretability.

During pilot experiments, microscopists typically attempt to increase the signal and decrease background noise from the sample. This is accomplished by selecting fluorophores to optimize photostability and brightness while minimizing spectral overlap with auto-fluorescence and using dye targeting strategies to optimize specificity and density of labelling while maintaining biological function. Microscopists also tune their measurement parameters, seeking to identify an illumination intensity that results in sufficient SNR to observe their target of interest over a sufficiently long duration, applying filters that cut out autofluorescence while keeping signal, and using optical sectioning to remove out-of-focus fluorescence.

Computational approaches offer additional, synergistic ways to boost the SNR through denoising images after they are collected or by dynamically tailoring the exposure during a measurement. There are also computational methods to reduce background fluorescence, for example, subtraction of a constant background or subtraction of local background in the special cases of isolated objects (for example, via top-hat filtering) or single molecules²². Here, we

review methods focused on SNR enhancement rather than on background removal.

Classical algorithms for computational denoising

Once sample labelling has been optimized, computational denoising can further improve the SNR (Fig. 1b). The simplest forms of denoising combine the signal from neighbouring pixels by binning them via a mean or median operation. Binning is fast and freely and easily accessible via open-source software packages such as Fiji²³. However, it sacrifices spatial resolution in favour of an improved SNR; other filtering-based methods, such as median filtering²⁴, maintain pixel resolution while still reducing noise.

More sophisticated methods that make a priori assumptions about the sample, such as total variation regularization²⁵ or non-local means²⁶, can be powerful for denoising but require careful, and often manual, parameter tuning. As one such example, by assuming the sample is spatially continuous within the resolution limit and temporally continuous over multiple frames (in other words, smooth in space and time), Hessian structured illumination (SIM) reconstruction²⁷ allowed 2D super-resolution imaging at roughly one-tenth the illumination dose typically required. This improved sensitivity permitted the capture of approximately 10 times more time points than previously possible, enabling the study of highly dynamic endoplasmic reticulum loops and exocytic fusion intermediates as well as cytoskeletal remodelling on the hour timescale²⁷.

Deep learning algorithms for computational denoising

Currently, the most potent denoising methods are based on deep learning algorithms²⁸ (Box 1 and Figs. 1b and 2), which use artificial neural network architectures. In supervised methods, pairs of low-SNR and corresponding high-SNR ground truth examples are provided as network training data. Millions of network parameters are adjusted during the training procedure as the network ‘learns’ to map from low-SNR images to predict the equivalent high-SNR images. The trained network can then be applied to previously unseen noisy data to generate a higher SNR prediction. Since information about the underlying data is incorporated into the network during training, such approaches can quantitatively outperform classical, data-agnostic denoising methods (Box 2 and Fig. 2), with important caveats (Box 3).

Since the illumination intensity can be lowered 10–100 times with the application of deep learning-based denoising^{11,29–32}, the increased photon budget may be spent in ways that enable fundamentally new measurements. For example, content-aware restoration (CARE)¹¹ predicted high-SNR images from noisy and otherwise hard-to-analyse spinning disc confocal microscopy images of nuclei in the planaria *Schmidtea mediterranea*, a flatworm with extreme sensitivity to light. It also improved the segmentation of noisy nuclear images in the developing beetle *Tribolium castaneum*. CARE works by training a neural network on pairs of images that represent the same object captured at a low SNR and high SNR. Whenever such training pairs of images can be acquired, CARE-based image denoising and restoration are applicable.

Denoising data from more advanced microscope setups, such as classical 2D-SIM³³ and 3D-SIM¹⁶ as well as lattice light-sheet microscopy-based SIM³⁴, has also used deep learning. A different network architecture, that is, a residual channel attention network (3D-RCAN), was designed to denoise 3D volumetric data from fluorescence microscopy²⁹. Denoising low-SNR instant SIM (iSIM)³⁵ recordings of mitochondria in living U2OS cells enabled the collection of 2,600 super-resolution volumes without detectable photobleaching

Box 1

Deep learning

Deep learning is a popular field in machine learning that uses artificial neural networks (ANNs) to learn complex functions from data. When suitable data is available, large (deep) ANNs can learn to become powerful predictors, capable of outperforming all other known methods in a plethora of tasks, for example, image classification, denoising, super-resolution or segmentation.

An ANN is a sequence of layers containing nodes analogous to neurons and connections between nodes in neighbouring layers. Each connection between two nodes has a weight, roughly modelling a synapse between two neurons. During training of an ANN, typically only those weights are changed and connections are not added or removed.

Supervised from self-supervised and unsupervised training is distinguished depending on what data is available or required to train an ANN. Data for supervised training comes in pairs of inputs and corresponding desired output or prediction (ground truth). The availability of ground truth allows computing of the error, referred to as the loss, between the current prediction by the network and the desired result (ground truth). A technique known as error backpropagation enables changing of all weights in the network in such a way that the same input will lead to a prediction that is closer to the ground truth that the loss was computed against. Hence, if training is successful, the loss will diminish over time and the ANN predictions will become better. Training data must be collected in addition to data for validation of ANN performance or interpretation in a study. This is done to make sure that the network has generalized to the data type and to avoid ‘overfitting’, in which weights are tuned to features specific to the training set. The size of a training dataset varies and may lie between tens and hundreds of images or image stacks.

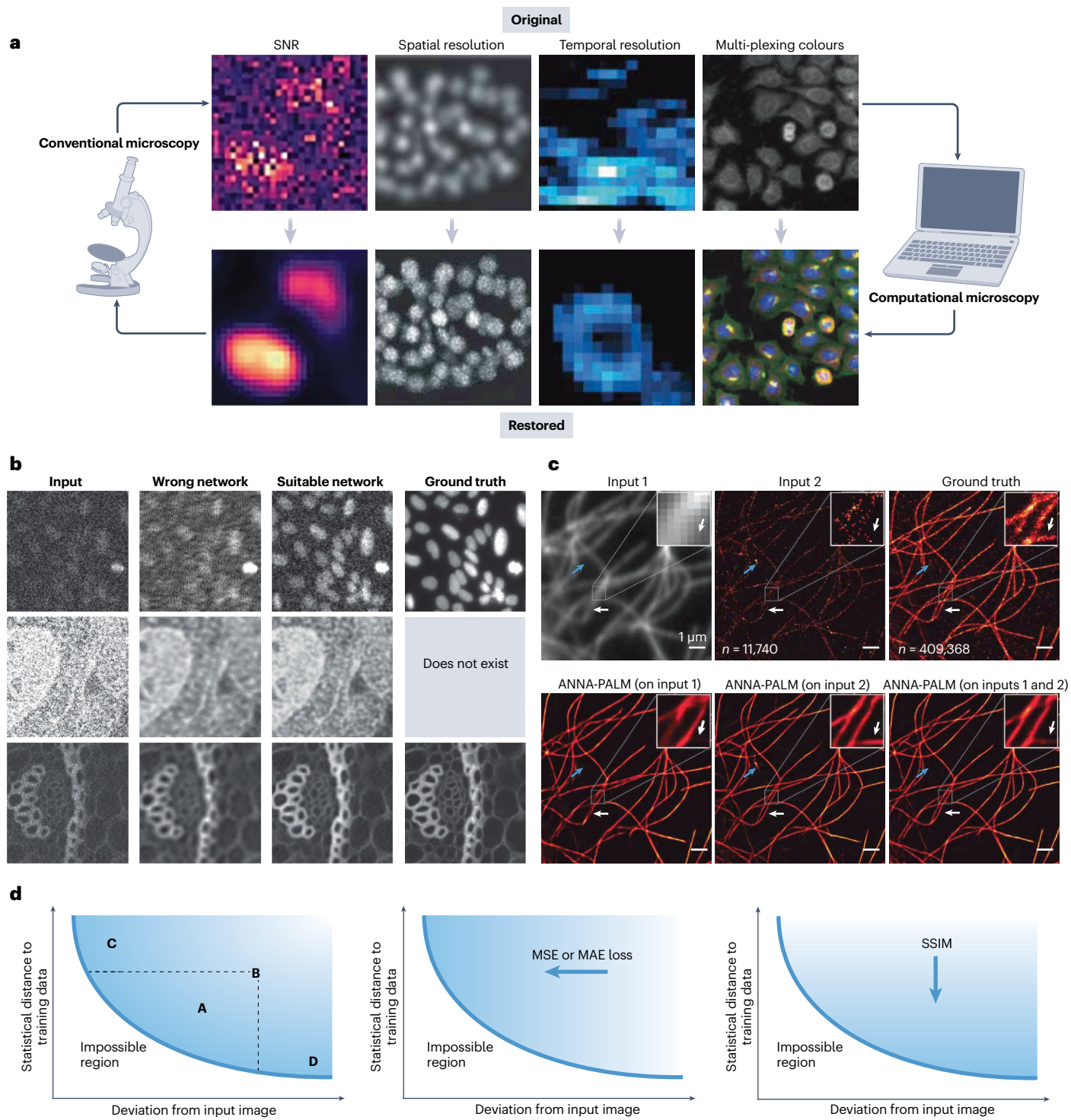
Self-supervised or unsupervised training, in contrast, does not need the user to provide ground truth data, making such approaches easier to apply. For example, self-supervised methods may change or hide some aspects of the available data and ask the ANN to predict those aspects. Masking single pixels and then asking a network to predict the intensities of the masked pixels trains rather powerful denoising networks; no ground truth is required and the original image data is enough to self-supervise the network on the desired task. While such approaches are highly sought after, for tasks other than denoising and segmentation, they remain to be developed (see also Box 3).

If interested readers would like to dive deeper into the details of deep learning in the context of tasks relevant to biologists, see ref. 120 for a review.

or photodamage, improving experiment duration by several orders of magnitude. This imaging duration and gentleness are reminiscent of those attained with light-sheet microscopy, but the denoised iSIM volumes afford higher resolution.

In a further example, knowledge of the physics of image formation was combined with denoising to yield high-quality reconstructions³²

Review article



with fewer artefacts than previous methods. This method was used to resolve the fast kinetics of beating cilia and intraflagellar transport, the rapid interactions between membrane-bound and membrane-less organelles, and the assembly and disassembly of nucleoli within mitotic cells³² – all applications that would have been difficult or impossible to observe without powerful denoising methods.

Adaptive illumination to increase SNR

Microscopists often attempt to find the minimum excitation intensity that will achieve a desired SNR to avoid photobleaching and phototoxicity. However, expression levels and local concentrations of different proteins may differ by orders of magnitude; thus, each structure in a cell or tissue can have a different optimal excitation intensity. Moreover,

Review article

Fig. 1 | Live-cell imaging and deep learning: overview, examples and limitations. **a**, Schema of conventional and computational microscopy. The finite photon budget constrains live-cell imaging, resulting in conventional microscopy images with limited signal-to-noise ratio (SNR), spatiotemporal resolution or spectral bandwidth (top row). Computational microscopes can circumvent these limitations by using image processing (for example, deep learning-based denoising) to enhance the raw image data (bottom row) or by using computation to acquire better data to begin with (for example, by using feedback from the analysis to adapt the acquisition to iteratively improve SNR or resolution). **b**, Example of unsupervised computational denoising. A Noise2Void¹⁸ artificial neural network (ANN) was trained either on data dissimilar to the input data (wrong network) or on data similar to the input data (suitable network), for three different sample types (rows). The network outputs obtained for the same input are shown. High-SNR ground truth is not required to train these unsupervised models, which only require sufficient amounts of suitable training data, and for the data in the second row, high-SNR ground truth does not even exist. Training the ‘wrong network’ with a mean squared error (MSE) loss results in a blurry predicted image because of structural mismatches between the training and input data. However, a ‘suitable network’ can denoise without obvious artefacts. **c**, Deep learning for super-resolution. ANNA-PALM is an ANN (Box 1) trained on widefield and photo-activated localization microscopy (PALM) images. Top row: widefield (input 1) and two PALM images, created by collecting a few (input 2, $n = 11,740$) or many more (ground truth, $n = 409,368$) single-molecule events. Bottom row: ANNA-PALM predictions obtained by providing the network with either one or both input images. Arrows point to errors in ANNA-PALM predictions, blue arrows indicate errors when input 1 is provided, and white arrows indicate errors when one or both inputs are provided. Predictions become more similar to the ground truth when more inputs are

provided. Figure adapted from ref. 119. **d**, Deep learning-based image restoration and its limitations. Computational microscopy includes image restoration methods, which attempt to improve some aspect of lower-quality raw image data by making it more similar to higher-quality training data, the ground truth image or both (shifting it towards a bluer area). In these plots, any ANN-predicted image can be represented by a single point, whose distance along the y-axis represents its statistical distance to the training data, and whose distance from the x-axis represents its deviation from the input image. Since noisy or distorted images have lost information compared to ground truth, they cannot be fully restored; no ANN can perfectly predict the ground truth giving rise to an ‘impossible region’ beyond the blue line. ANN predictions will depend on how the training is conducted. Predictions will tend to be more similar to the input data (pushed towards the y-axis) when using MSE or mean absolute error (MAE) losses as in content-aware restoration or Noise2Void methods (middle plot), or they will tend to be more statistically similar to structures contained in the training data when a structural similarity index measure (SSIM) is used (rightmost plot). The blue arrows and colour gradients show the direction towards which models flow when different losses are optimized during network training. How do the four models A, B, C and D (leftmost plot), representing outputs of different ANN, compare against each other? Model A is better than model B in both dimensions since it is closer to the origin (within the dashed lines representing the coordinates of B), but which of the models A, C and D is ‘better’ depends on whether the user wishes to recover an image most like the input image, to generate an image most similar to the training data, or something in between. Part **a**, right, reprinted with permission from ref. 101, AAAS. Part **a**, middle right, reprinted from ref. 94, Springer Nature Limited. Part **a**, left, adapted from ref. 11, Springer Nature Limited. Part **a**, left middle, provided by H.S. Part **b** provided by F.J. Part **c** reprinted from ref. 119, Springer Nature Limited.

biological samples are heterogeneous in space and time, implying that illumination patterns designed to achieve a uniform SNR would be non-uniform in space and time. For example, regions with fluorescence below a threshold value – implying no signal of interest – could be skipped over, while regions with fluorescence above the threshold could be illuminated to maintain a given SNR. Such decisions can be delegated to an automated microscope controller, which may be faster and more accurate than a human. In this manner, coordination between the sample fluorescence and the microscope hardware components through a feedback loop can execute complex acquisitions.

Adaptive illumination strategies based on feedback between the sample and hardware have been demonstrated in different microscopy modalities, from conventional to super-resolution approaches. Controllers for point-scanning confocal microscopy³⁶, two-photon microscopy^{37,38}, stimulated emission depletion (STED) microscopy³⁹ and SIM⁴⁰ have been designed to automatically tune the illumination intensity according to the amount of detected fluorescence. This adjustment is typically achieved on the picosecond timescale and can be conducted locally point-by-point as the illumination is scanned across the sample.

Reducing the sample exposure to focused light is particularly important for STED microscopy, where fluorescent molecules are exposed to the high intensities of the depletion doughnut, increasing the risk of photodamage. If no photons are detected in a sample location, RescueSTED³⁹ assumes that no fluorescently labelled structures are present, and switches the depletion laser OFF while moving to the next point in the sample. More advanced versions, named MINFIELD⁴¹ or DyMIN⁴², increase the depletion intensity only when a structure is centred to provide the maximum spatial resolution on structures of interest. This adjustment minimizes exposure of the fluorescent

molecules to the high intensities of the doughnut crests and allows photobleaching reduction up to 100-fold.

Light exposure in point-scanning systems is determined by laser intensity and dwell time. To reduce unnecessary illumination, feedback loops can tell the scanner to illuminate a certain region of the sample until the desired SNR is reached as adopted in smart reversible saturable optical fluorescence transitions (RESOLFT)⁴³ and Hopping STED⁴⁴ microscopes. This allowed peroxisomes and mitochondria to be imaged at up to 30 frames per second in cultured cells and actin rearrangements to be imaged at a depth of 20–30 µm inside a developing *Caenorhabditis elegans*. Automatic re-adjustment of the illumination in a sample-adaptive manner has also been beneficial for single-molecule localization microscopy⁴⁵, where the photo-activation light was dynamically adapted to achieve efficient recording of sequential single-molecule events.

Real-time feedback as described here is an advanced approach, and thus far has only been applied to limited cases and methods where photobleaching is consistently a major concern such as in super-resolution microscopy. However, such feedback methods are becoming increasingly accessible as microscopists, core facilities and commercial developers aim to execute more complex acquisitions^{46–51}.

Improving spatial resolution

Blurring of the image introduced by light diffraction results in a fundamental information loss when the underlying sample is imaged with any fluorescence microscopy modality. Subcellular structures are frequently of interest but are most affected by blurring since their dimensions are typically near or below the diffraction limit. Thus, methods that reverse spatial blur-induced loss of resolution are of great value for biological imaging. In 2014, the Nobel Prize in Chemistry

Review article

Table 1 | Summary of methods

Method	Type	Advantages	Requirements/ assumptions	Drawbacks, potential artefacts	Proof-of-concept method and/or imaged sample	Availability
Denoising						
Binning	CL	Simple	Object is oversampled by the detector	Reduction in the spatial resolution	General	Common (ImageJ, FIJI, and so on)
Median filtering ²⁴	CL	Simple	Intensity of each pixel is related to that of its neighbours	Smooths signal, removes edges	General	Common (ImageJ, FIJI, and so on)
Total variation regularization ²⁵	CL	Preserves edges of objects in the image	Noise corresponds to excessive variation in the image	Creation of patches of pixels with the same intensity/staircase artefacts'	General	For example, existing Scipy function (<code>denoise_tv_chambolle</code>)
Non-local means ²⁶	CL	Considers values of other pixels in the image	User-defined weighting function that relates different pixels	Computationally expensive	General	Fiji nlm Napari nlm Skimage nlm
Hessian SIM ²⁷	CL	Effective at very low SNR	Assumes spatial and temporal continuity of objects	Computationally expensive	2D-SIM; used for visualization of organelles, cytoskeleton	GitHub pycudasirecon
Content-aware restoration ¹¹	DL (supervised)	With proper training, one can expect resolution improvements of ~twofold to threefold over input; can denoise so that illumination intensity can be lowered by more than -tenfold over conventional imaging	Requires training data	Fails, especially at ultra-low input SNR (<3) or >twofold resolution enhancement; depending on the method, results are either blurry or cause hallucinations (for example, in background regions); slow to train (hours, longer than image acquisition); quality of results depends on similarity between data and training data	Used for visualization of small organisms, tissues, cytoskeleton	CSBDeep GitHub CSBDeep
Residual channel attention network restoration ²⁹					Used for 3D visualization of organelles, cytoskeleton, chromosomes	GitHub 3D-RCAN
Deep Fourier channel attention network restoration ³¹					2D-SIM; used for visualization of cytoskeleton, organelles	GitHub DL-SR
Point-scanning super-resolution ³⁰		Effective for under-sampled, noisy data	Point-scanning data, training data		Confocal, electron microscopy; used for visualization of organelles	GitHub PSSR
Rationalized deep learning ³²		Improves prediction uncertainty	Prior knowledge of illumination patterns, training data		2D-SIM, 3D lattice light-sheet; used for visualization of cytoskeleton, organelles, chromosomes	GitHub rDL-SIM
Noise2Void	DL (unsupervised)	Removes pixel noises (for example, Poisson and Gaussian readout noise), no training or low-noise data required	Noise must be pixel-independent	All spatially correlated signals are retained, including imaging artefacts	General	FIJI n2v Napari n2v GitHub n2v
Controlled light exposure microscopy ³⁶	CL+H	Improves SNR at reduced excitation light dose	High-signal regions are the most important	Relative intensities in different areas are difficult to interpret	Confocal; used for visualization of cytoskeleton and organelles	None
Spatial resolution						
Richardson–Lucy deconvolution	CL	Improves contrast and SNR	Point spread function is a user input, assumed constant across image	Too many iterations lead to over-sharpening; light and dark rings may appear around objects	General	Common (ImageJ, FIJI, and so on)

Review article

Table 1 (continued) | Summary of methods

Method	Type	Advantages	Requirements/ assumptions	Drawbacks, potential artefacts	Proof-of-concept method and/or imaged sample	Availability
Spatial resolution (continued)						
Sparse-SIM ⁵⁸	CL	Increases resolution at high frame rate	Sparsity and continuity of structures	Distortions and intensity fluctuations at low SNR	SIM, spinning disk confocal; used for visualization of cytoskeleton, organelles	GitHub Sparse-SIM
Richardson–Lucy network ⁵⁹	DL (supervised)	Improves performance axially and at low SNR, faster computation	Assumes that Richardson–Lucy is a good model for deconvolution, training data	Distortions at lowest SNR	Used for visualization of tissues, embryos, cells	GitHub Richardson–Lucy-Net
Cross-modality super-resolution ⁶⁵	DL (supervised)	High-resolution modality from low resolution	Information within low-resolution images is sufficient, training data	In the absence of sufficient information in low-resolution images, network may generate hallucinations	Confocal, STED; used for visualization of cytoskeleton, organelles	Fiji/ImageJ plugin
3D-SIM restoration ⁶⁶	DL (supervised)	Restores axial resolution based on higher-resolution lateral views	Objects should appear similar when viewed laterally or axially, training data	Time-consuming to collect volumetric data and train, prone to distortions at low SNR	3D-SIM; used for visualization of bacteria, cytoskeleton, organelles	GitHub SIMreconProject
Multiphoton adaptive optics ⁷²	CL+H	Corrects aberrations for deep imaging	Indirect wavefront sensing of aberrations	Setup includes expensive lasers; sensing slower than image acquisition	Multiphoton; used for visualization of mouse brain	GitHub JiLabAO GitHub Prevedell-lab/AO
SIM adaptive optics ⁷⁴	CL+H	Corrects aberrations for deeper super-resolution	Indirect wavefront sensing of aberrations	High level of user expertise	SIM; used for visualization of <i>Caenorhabditis elegans</i> , plants and animal cells	GitHub Knerlab
Multiphoton SIM adaptive optics ⁷⁵	CL+H	Corrects aberrations for deeper super-resolution	Direct wavefront sensing of aberrations	Setup includes expensive lasers; sensing ~1s or longer; point-scanning acquisition is slow	Multiphoton iSIM; used for visualization of embryos and cells	None
PHASENET ⁷⁶	DL (supervised)	Corrects aberrations for deep imaging	Aberration estimation from synthetic data, training data	Only demonstrated on beads	Confocal, widefield; used for visualization of synthetic beads	GitHub phasenet
MINFLUX ⁷⁹	CL+H	Requires fewer photons to localize molecules	Single molecules are isolated	High level of user expertise; complex optical setup	Specialized microscope; used for visualization of small molecular structures	None
AutoPilot ⁸²	CL+H	Matches excitation and imaging planes in real time	Sample changes between time points are small	High level of user expertise; complex optical setup	Specialized microscope; used for visualization of embryos	GitHub AutoPilot
Learned adaptive multiphoton illumination ⁸³	DL+H (supervised)	Optimizes local excitation in 3D sample	Requires specific calibration dataset for training, training data	High level of user expertise; strong reliance on model	Multiphoton; used for visualization of lymph node tissue	Zenodo Henry Pinkard (2020)
Temporal resolution						
Multi-focal SIM ⁸⁷	CL+H	Several cells thick, 1Hz imaging speed	Access to custom or commercial microscope	Complex optical setup	Specialized microscope; used for visualization of embryos, cells, cytoskeleton	Google Code msim
Spinning disk confocal image scanning microscopy ⁸⁸	CL+H	Implemented on commercial microscope, 1–3Hz imaging speed	Advanced programming capability	Customized control software	Spinning disk; used for visualization of cytoskeleton and molecular complexes (nuclear pore complexes, Tau protein aggregates)	None

Review article

Table 1 (continued) | Summary of methods

Method	Type	Advantages	Requirements/ assumptions	Drawbacks, potential artefacts	Proof-of-concept method and/or imaged sample	Availability
Temporal resolution (continued)						
iSIM ³⁵	CL+H	Real-time optical image processing, 100Hz imaging speed	Access to custom or commercial microscope	Complex optical setup	Specialized microscope; used for visualization of embryos, cells, cytoskeleton and organelles	Google Code msim
Parallelized RESOLFT ⁹³	CL+H	Higher resolution, 1Hz imaging speed	Reversibly switchable fluorophores	Complex optical setup; sensitive to crosstalk	Specialized microscope; used for visualization of cytoskeleton	Image reconstruction software included in ref. 93
3D parallelized RESOLFT ⁹⁴	CL+H	Higher resolution, 1–2Hz imaging speed, 3D	Reversibly switchable fluorophores	Complex optical setup	Specialized microscope; used for visualization of cytoskeleton, synaptic proteins, organelles	Acquisition software available at GitHub Testa Lab
Multiphoton 3D random access scanning ¹¹⁷	CL+H	Thick samples (~1mm), 100Hz time resolution	Sparse regions of interest	Complex optical setup and control software	Specialized microscope; used for visualization of synaptic activity in brain slices	Included in ref. 117
Event-driven acquisition ⁹⁷	DL+H	On-demand shift in frame rates	Events of interest are rare and have precursors, training data	Measurement bias towards events detected by network; complex setup	iSIM widefield; used for visualization of organelles and bacterial cells	Micro-manager EDA plugin
Event-triggered STED	DL+H	On-demand shift from widefield to STED	Events of interest are rare and have precursors, training data	Measurement bias towards events detected by network; complex setup	STED; used for visualization of organelles	GitHub etSTED
Multi-colour imaging						
Learning unsupervised means of spectra ¹⁰³	DL (unsupervised)	No pre-knowledge needed of fluorophores	Each pixel contains only one fluorophore, emission spectra share same shape	Up to six fluorophores	Multiphoton; used for visualization of cytoskeleton and organelles	Figshare for ref. 103
Phasor spectral fluorescence lifetime imaging microscopy ¹⁰⁷	CL	Avoids fitting to retrieve fluorescence lifetime, no pre-knowledge needed of fluorophores	Fast electronic card for photon counting	Complex hardware; customized analysis pipelines	Fluorescence lifetime imaging microscopy; used for visualization of organelles	Included in ref. 107
UNMIX-ME (multiple emissions)	DL (supervised)	Combines spectral and lifetime signatures	Synthetic training data, knowledge of spectra required	Requires a combination of Matlab and Python (Tensorflow)	Fluorescence lifetime imaging microscopy; used for visualization of organs	GitHub UNMIX-ME

CL, classical type; DL, deep learning; H, hardware; iSIM, instant structured illumination microscopy; RESOLFT, reversible saturable optical fluorescence transitions; SIM, structured illumination microscopy; SNR, signal-to-noise ratio; STED, stimulated emission depletion.

was given for a family of ‘super-resolution’ microscopy methods that cleverly circumvent the diffraction limit. These techniques, which differ considerably in practical implementation, have been reviewed extensively elsewhere⁵². We note that these methods make no assumptions about the sample structure but have tradeoffs – the greater the resolution gain, the higher the cost in SNR, phototoxicity or temporal resolution – making some better suited for live imaging than others⁵³.

In this section, we describe computational strategies that alleviate these tradeoffs, deconvolution and deep learning methods that

enhance the resolution and contrast of the raw data, adaptive optics methods to maintain resolution in thicker samples such as tissue, where aberrations distort the light, and real-time feedback methods to achieve improvements in spatial resolution without sacrificing SNR or sample health.

Deconvolution

The blurring introduced by fluorescence microscopy can be considered analogous to a low-pass filter, in that the microscope transmits

all spatial frequencies up to the resolution limit. Low spatial frequencies (corresponding to larger features in the sample) are transmitted at higher SNR than high spatial frequencies, leading to a resolution-dependent loss in contrast that can obscure fine details in low-resolution haze, particularly for 3D samples (which suffer from greater out-of-focus background). Fortunately, if the blurring function and noise characteristics of the microscope are well characterized, this degradation of image quality can be partially reversed using a computational procedure known as deconvolution⁵⁴ (Fig. 3a–c). The main practical benefit is a large improvement in contrast and SNR, which in turn leads to discernible improvements in spatial resolution over the raw input data.

The deconvolution literature is vast, and properly surveying it would require a separate review. Where should a new user begin? Classical deconvolution algorithms are still effective and remain broadly used. For example, the decades-old Richardson–Lucy^{55,56} algorithm iteratively deblurs an estimate of the sample given a known point spread function and assumed Poisson noise (which is usually dominant in fluorescence microscopy)⁵⁷.

Deconvolution methods that incorporate additional information about the specimen can considerably improve upon the Richardson–Lucy algorithm, in some cases restoring fine detail outside the classical resolution limit. This is accomplished either by assuming an underlying smoothness²⁷ or sparsity⁵⁸ to the sample, or by explicitly incorporating sample information into deconvolution via deep learning⁵⁹. Such improved performance comes at a cost, requiring either careful parameter tuning^{27,58} or training data⁵⁹.

Finally, deconvolution can be used beyond its ‘traditional’ context in deblurring images captured with conventional fluorescence microscopes. Deconvolution is often at the heart of ‘computational microscopes’, including multi-view light-sheet^{60,61} or confocal⁶² imaging systems that improve volumetric resolution and SNR by jointly using information from each view to increase their resolution to the best among them. Deconvolution can also be used to combine information from different microscopes⁶³ – enabling, for example, kiloHertz activity imaging of acetylcholine and voltage deep in mouse brain with rapid line-scanned multiphoton tomography after first acquiring a static high-resolution volume with traditional raster-scanned multiphoton microscopy⁶⁴.

Deep learning-based resolution enhancement

In contrast to the ‘classical’ super-resolution techniques mentioned above, resolution enhancement can also be enabled by embedding prior knowledge about the structure of a sample into a trained neural network, with some important caveats (Box 4). By acquiring matched low-resolution and high-resolution training data, such ‘cross-modality’ resolution enhancement neural networks have improved the spatial resolution of total internal reflection fluorescence⁶⁵ and widefield³¹ microscopy using SIM ground truth, of confocal microscopy using line-scanning SIM⁶² and STED microscopy ground truth^{29,65}, and of instant SIM using expansion microscopy ground truth²⁹. Although none of these methods perfectly reproduces the higher-resolution modality, the main benefit is that resolution is enhanced while retaining the higher acquisition speed, SNR and/or phototoxicity advantages of the lower-resolution method (Fig. 3d,e). Even greater benefits accrue when using multistep networks trained to sequentially denoise and enhance resolution^{29,62,66}. As examples, these methods have revealed mitochondrial nucleoid dynamics in the context of mitochondrial cristae and the rotational

streaming of mitochondrial tubes³¹; mitochondrial fission³⁰, cell division²⁹ and cytoskeletal dynamics within immune cells^{29,66}; and subcellular growth cone dynamics in living *C. elegans* embryos⁶². The inferred high-resolution images can enable more accurate segmentation and reveal finer detail than lower-resolution raw data.

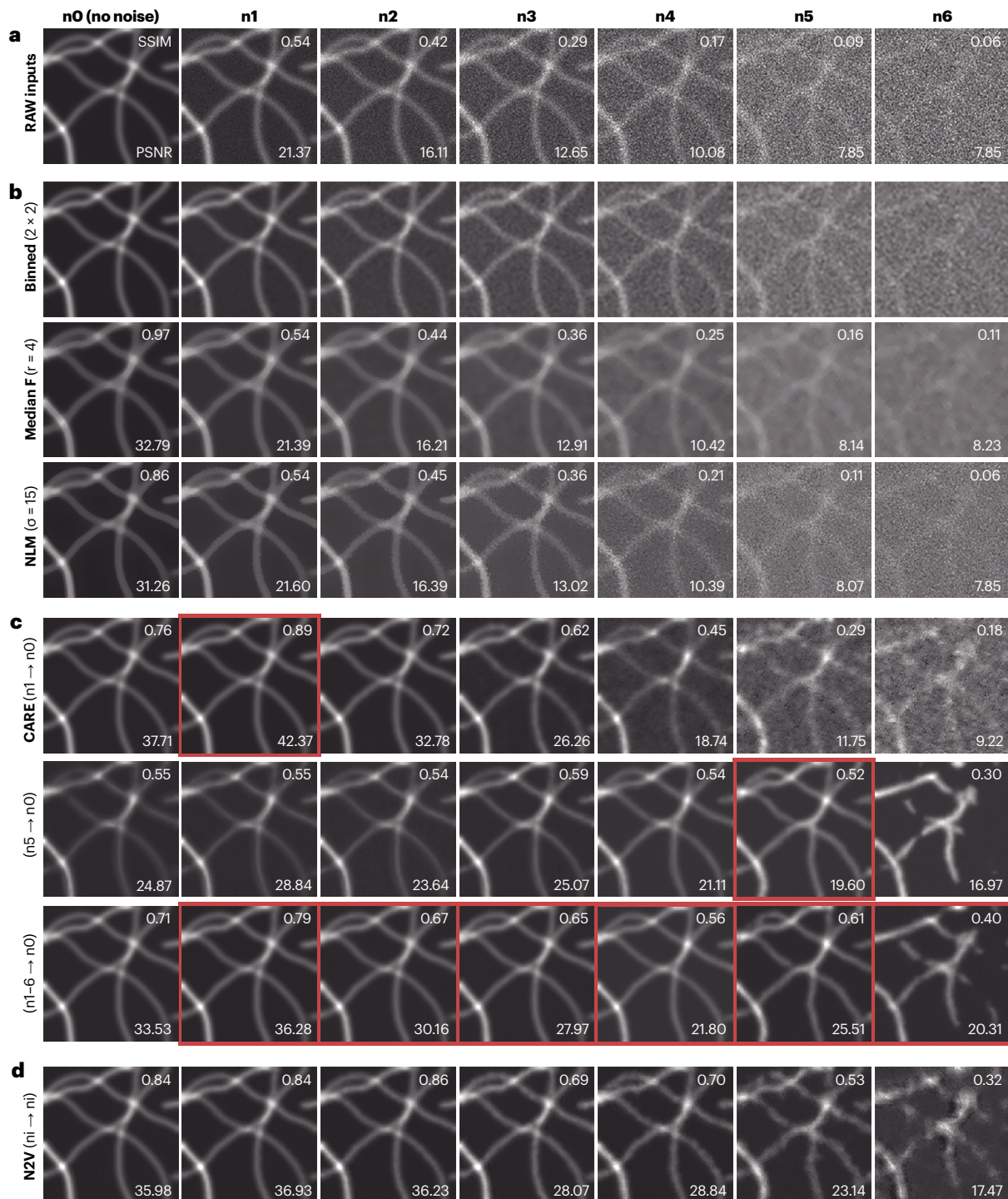
Deep learning can also compensate for the anisotropic point spread function present in most optical microscopes^{11,67}, which results in twofold to threefold worse resolution axially along the optical axis than laterally in the imaging plane. The concept is to create isotropic image volumes by blurring and downsampling image stacks in the lateral dimension so that lateral views resemble the axial data recorded by the microscope. A neural network can reverse this degradation to improve resolution in the axial views given the high-resolution lateral ground truth from the original images and the assumption that structures look similar in both axial and lateral views. This method has been applied to volumetric data from fruitfly wing or whole embryo, zebrafish eye, and mouse liver; in the fruitfly embryo case, leading to an increase in resolution sufficient to quantitatively improve nuclear segmentation¹¹. Similar concepts have been used to improve isotropy in multi-view confocal super-resolution microscopy⁶², revealing dynamic histone nanodomains in live Jurkat T cells and offering clear views of the nerve ring region in anaesthetized larval *C. elegans*, as well as in 3D-SIM, enabling high-contrast volumetric time-lapse imaging of organelle dynamics at 120 nm isotropic resolution⁶⁶.

Adaptive optics to correct spatial aberrations

High-resolution or super-resolution imaging is much easier to achieve in single cells than in tissue, in part because thicker samples contain more interfaces and subregions that can bend light. Such bending can significantly distort the wavefront of light, causing optical aberrations that prevent diffraction-limited focusing, reducing spatial resolution, contrast and SNR. Given the importance of studying living cells away from the coverslip in a more physiological context, adaptive optics methods^{68,69} that can measure and subsequently correct the aberrated wavefront are of great value.

The key challenge in the use of adaptive optics is determining the aberrated wavefront; once known, the aberration can be corrected by a deformable mirror or spatial light modulator programmed to apply an equal and opposite aberration. Methods can be broadly classified as ‘direct’ or ‘indirect’. Direct methods introduce point sources with known emission profiles and use dedicated hardware to sense deviations from the expected diffraction-limited emission. Indirect methods iteratively estimate the wavefront by applying known aberrations while monitoring an image quality metric. Direct wavefront sensing tends to be faster, while indirect methods are better suited to imaging in opaque tissue; both have been applied to substantially improve image quality in live imaging studies conducted with confocal⁷⁰, light-sheet⁷¹, multiphoton^{72,73} and structured illumination^{74,75} microscopy.

Despite these successes, existing implementations of adaptive optics also introduce more illumination dose, degrade temporal resolution, and add substantial complexity as well as financial cost relative to the base microscope they are designed to enhance. These issues have hindered the widespread adoption of adaptive optics and have confined it to the province of relatively few labs. Improving the performance and accessibility of adaptive optics is an important frontier in computational microscopy and could have an outsized impact given that the vast number of microscopes suffer from increasing depth-dependent aberrations. Although existing efforts are nascent^{76–78}, we suspect that deep learning could have an important part to play in the future.



Real-time feedback and inference of sample properties to enhance spatial resolution

Feedback loops that link sample-based computation to the microscopy hardware for adaptive acquisitions can be used to enhance spatial resolution. One such example is MINFLUX microscopy⁷⁹, which reduces the number of photons required to localize single molecules. This is enabled by sequential, patterned illumination of isolated fluorophores,

coupled with real-time computation to infer their positions. In response to the estimated position, the microscope re-positions the illumination pattern, thereby localizing the emitter with a precision of a few nanometers. This technique outperforms the standard method of uniform illumination followed by centroid finding with orders-of-magnitude fewer photons. With this efficient use of the photon budget, the individual steps and rotations of single motor proteins could be tracked in three

Fig. 2 | Comparison of denoising methods. **a**, Synthetic raw input image without noise (n_0) and with varying levels of added noise (n_1 – n_6). The noise-free image is also the reference image to compute structural similarity index measure (SSIM) and peak signal-to-noise ratio (PSNR) values for all applicable images in this figure (see Box 2 for details). **b**, Denoising results obtained via some classical methods described in Table 1: 2×2 pixel binning (top row), median filtering with a radius of 4 pixels (middle row), and non-local means (NLM) using a value of 15 for the standard deviation of the noise distribution (bottom row). All methods appear effective for low values of noise (n_1 , n_2) but begin to degrade for intermediate values (n_3 , n_4) and are ineffective for high values (n_5 , n_6). **c**, Denoising results obtained with the supervised deep learning method content-aware restoration (CARE), which uses pairs of high-SNR and low-SNR images as training data. The three rows represent different CARE models, all trained on the same noise-free images as ground truth but using different noise levels for the low-SNR image

(red boxes): the top row uses n_1 paired with n_0 , the middle row uses n_5 paired with n_0 , and the bottom row uses each level of noise in turn (n_1 – n_6) paired with n_0 . Training the network on noisier images allows it to better denoise noisier images, although its performance becomes slightly degraded for less noisy images. A better all-around performance at different noise levels is achieved with the model that was trained on all levels of noise. **d**, Denoising results obtained with the self-supervised method Noise2Void (N2V). Each column shows the result obtained with a N2V network trained on this noise level specifically (no ground truth is required, except to compute (PSNR) values). Supervised training (Box 1) typically leads to better results whenever training data similar to the input data is available and used. Since unsupervised methods can be trained on the same body of data to be denoised, generating suitable training data should not be a problem. Images in this figure were provided by F.J.

dimensions in vitro and in cells, at physiological ATP concentrations^{80,81}. MINFLUX has the potential to make localization microscopy more compatible with time-lapse imaging, although bottlenecks remain related to the need for high-density labelling to resolve structures, the label size of which often exceeds the nanometric localization precision, and the difficulty of isolating individual fluorophores.

Light-sheet microscopy, while among the gentlest microscopy approaches, can also make use of feedback loops to increase image quality. The AutoPilot⁸² framework dynamically adapts properties such as light-sheet intensity and position to maximize focus and contrast in real-time, even as the imaged embryo undergoes major changes in size, fluorophore expression, concentration and positioning during organogenesis.

Artificial neural networks can enhance the performance of data-driven microscopy control by aiding decision-making in complex settings. In learned adaptive multiphoton illumination⁸³, a trained neural network selects illumination intensities while imaging 3D scattering samples such as lymph nodes. Here, the choice of illumination intensity is based on a complex relationship between fluorescence intensity, incident excitation power and fluorophore spatial distribution. Automated tuning of imaging parameters was also guided by machine learning for STED and confocal imaging to enhance image quality by optimizing laser power and pixel dwell time⁸⁴.

Improving temporal resolution

The temporal resolution of a time-lapse microscopy experiment is defined as the amount of time between images. It is also characterized by the imaging speed or frame rate, which is typically reported as the number of frames per second or, equivalently, Hertz. In microscopy, the minimum value of the temporal resolution is the time it takes to acquire a single image. For dynamic processes taking place on timescales that are slow compared to the time to acquire a single image, a delay between frames may be added, which is then also added to the temporal resolution. Without sufficient temporal resolution, biological processes can appear distorted by motion blur if objects move during the capture of a single frame, or can be missed altogether. A valuable concept for thinking about the measurement parameters needed to resolve a process is the Nyquist-Shannon sampling theorem, which defines the minimum spatial or temporal sampling rate required.

Time resolution is limited by the sample: proteins or other biomolecules of interest may be present in the cell at low abundance; thus, the sample must be exposed to enough light to achieve the desired SNR. This means that exposure times must be long enough or, in the case of

focused excitation, dwell times must be sufficient to gather enough photons at each location in the sample given that the fluorescence lifetime is typically a few nanoseconds. As a result, denoising (see ‘Improving the SNR’ above) can have the added value of reducing acquisition time, since noisier data can be collected more rapidly.

Hardware does not usually limit the time resolution when imaging 2D samples – for widefield illumination, detectors are cameras, and high-end cameras such as sCMOS (scientific complementary metal oxide semiconductor) sensors can achieve frame rates greater than 1,000 frames per second, much faster than most cellular processes. When using focused illumination, imaging speed depends on the time to scan the excitation pattern over the sample while maintaining sufficient SNR at each location. The detector is typically a photomultiplier with nanosecond response times; thus, for single-point measurements such as in fluorescence correlation spectroscopy of molecular diffusion, the time resolution is more than adequate. However, the acquisition time is scaled with the scanned sample area and is multiplied by the number of planes in volumetric imaging, which can often present a practical bottleneck that limits acquisition speed.

Parallelized scanning microscopes

Parallelization collects information from multiple sample areas simultaneously. Thus, it offers a means of increasing imaging speed by reducing the scan range needed to image a field of view. One approach for imaging rapidly in a single plane is to use multi-focal excitation such as in spinning disk confocal microscopy. Compared with point-scanning, the speed to record a field of view increases proportionally to the total number of foci in the disk. The emission from the foci is collected by a camera, allowing acquisition rates of several hundred frames per second. The main tradeoff compared with a point scanner is lateral and axial crosstalk, which can degrade SNR and optical sectioning in thick or densely labelled samples.

Several super-resolution techniques have taken a similar approach, boosting resolution through computational post-processing or optical image processing. Lateral resolution in confocal microscopy can be improved by detecting the fluorescence emission with a camera and reassigning the light to account for blurring due to off-axis detection⁸⁵. A similar gain in resolution can theoretically be achieved by closing down the pinhole of the confocal microscope, but image reassignment offers much higher SNR compared to this approach since light that would otherwise be rejected by the pinhole is collected and used; this reassignment⁸⁶ is available in some commercial microscopes (for example, the Zeiss Airyscan). A parallelized version (multi-focal SIM)

Box 2

Quality measures for deep learning-based methods in microscopy

In microscopy image analysis, accurately assessing the improvements made to images by classical methods or artificial neural networks is crucial. This box offers an overview of the most commonly used quality metrics, providing insights into what they measure and their appropriate applications.

Common quality measures are mean squared error (MSE), mean absolute error (MAE), peak signal-to-noise ratio (PSNR) and structural similarity index measure (SSIM). All four require clean (ground truth quality) images, corresponding lower-quality images, and their improved (for example, denoised) counterparts. The comparison of a restored image to the ground truth is meaningful only relative to the comparison of the corresponding unrestored image to the ground truth. For self-supervised methods, such as Noise2Void¹¹⁸, such ground truth data might not exist, rendering all four metrics inapplicable.

The MSE and MAE are simple, pixel-wise error metrics. MSE calculates the squared difference and MAE the absolute difference between the evaluated image (x) and the ground truth image (y). Lower values indicate a better match between the input and ground truth images and can be used to compare the performance of two artificial neural networks.

The PSNR expresses the ratio between the brightest pixel in y (or the brightest minus the darkest pixel in y) squared and the MSE between images x and y . The final PSNR value is then ten times the logarithm (base 10) of this number, which assures that the PSNR is positive. This metric has the advantage of putting the MSE, which

represents the noise of the restoration, into context since it is compared to the range of pixel intensity values. Higher values signify a higher-quality image restoration. In many publications, the PSNR implementation additionally allows for x to be shifted in intensity to minimize the MSE between it and the ground truth image y . This effectively adds a constant intensity to all pixels in x such that the computed PSNR is maximized and the structure in the image is evaluated rather than the absolute intensity values.

The SSIM was initially developed to measure the perceptual difference between two similar-looking images¹²¹. Explaining the details of this measure goes well beyond the scope of this box. Higher SSIM values signify better quality input images, with 1 being a perfect match between x and y (and -1 signifying perfectly anti-correlated images).

A more advanced form of the SSIM, called the multiscale SSIM, attempts to measure the SSIM over multiple spatial scales through a process of multiple stages of sub-sampling¹²² and is sometimes used in the context of microscopy data denoising or super-resolution.

Perceptual image quality metrics have recently become popular in the domain of natural images¹²³, but we do not recommend using such measures in the context of scientific image data where the perceptual similarity between images is less important than quantifiable similarity. In simple terms, a reconstructed or restored image that is convincingly similar to real data is not the goal of scientific image processing — rather, the goal, is to arrive at an image that is as close as possible to the ground truth of the particular image.

has also been invented, using an array of excitation beamlets^{87,88}, which enabled imaging of cytoskeletal microtubules and actin in 3D cultured cells and living zebrafish embryos at ~1 frame per second.

In re-scan confocal⁸⁹ and optical photon reassignment⁹⁰ microscopies, optical image processing performs the re-assignment in a single camera exposure. This concept has also been parallelized in the iSIM³⁵ and related solutions⁹¹, which take advantage of thousands of parallel excitation beamlets and matched detector pixels to achieve speeds of ~100 frames per second, with 3D optical sectioning performed by a pinhole array. Commercial solutions are available and standard fluorophores can be used, with photostability being a desirable quality. These methods all offer up to a twofold improvement in spatial resolution derived from photon reassignment and deconvolution (see ‘Deconvolution’ section).

The super-resolution method RESOLFT⁹² is also compatible with live-cell imaging and parallelization. Technically similar to STED in its use of a focused, scanned excitation laser and a doughnut-shaped depletion laser, RESOLFT microscopes rely on special fluorescent proteins as labels that can be turned off with gentler depletion or ‘off-switching’ intensities. As for every scanning microscope, the time to collect an image increases with the number of scan positions required, that is, with the size of the field of view. Parallelization has also been used to speed up and expand the field of view in RESOLFT microscopy by creating an array of more than 100,000 nanosized excitation and off-switching regions in the

sample recorded at the same time⁹³. This allowed intermediate filaments and cytoskeletal actin to be imaged in living cells at two frames per second, with resolutions below 100 nm. These nanosized excitation and off-switching volumes can also be confined axially and scanned to enable 3D super-resolution imaging in living cells⁹⁴. With this approach, actin filaments and mitochondrial networks were resolved volumetrically and their spatial organization was quantified in living cells.

Deep learning approaches to increase imaging speed

Many super-resolution methods are slower than diffraction-limited methods due to the time and light dose required to photoswitch fluorophores. Deep learning approaches can be used to increase the speed of data acquisition for these methods.

In some methods, a neural network attempts to directly predict a higher-resolution image from a single low-resolution input image, benefiting from the higher imaging speeds of lower-resolution methods such as widefield or confocal microscopy. Deep learning can also speed up acquisitions for single-molecule localization microscopy (SMLM)⁹⁵. SMLM pools localizations gathered from many diffraction-limited images of isolated molecules to generate a super-resolution image. Collecting sufficient localizations to sample the structures of interest takes hundreds or thousands of raw images, generally limiting the method to fixed cells. Allowing molecules to be fluorescent at higher densities, so that they are no longer isolated, speeds up sampling but

makes precise localization more challenging. Because single-molecule images are relatively simple to model, synthetic data can provide a large amount of training data in the absence of ground truth (molecular positions) for real data. The DECODE⁹⁶ network trained on synthetic data could predict molecule locations from high-density data, where multiple emitters were turned on simultaneously. This procedure detected more localizations with better precision than all previous approaches, while simultaneously lowering the number of raw data frames required to reconstruct an image. These advances improved the speed and lowered the phototoxicity of SMLM data collection (70% less illumination and 7 times faster than previously possible), thereby enabling the dynamics of the Golgi apparatus and endoplasmic reticulum to be reconstructed from 7.5 s of raw data and nuclear pore complexes from 3 s of raw data.

Sample-adaptive imaging speed

Dynamic changes in biological samples can be used to guide microscopy experiments without user intervention and prioritize using the limited photon budget to image rapidly on demand. This is especially valuable in the case of rapid or transient biological events.

For example, mitochondrial fissions occur intermittently every few minutes and proceed over a few seconds. When observed with techniques such as iSIM³⁵, which provide higher spatial resolution compared to conventional microscopy, photobleaching and phototoxicity limit the duration of the observation. In event-driven acquisitions⁹⁷, a neural network was trained to recognize mitochondrial precursors to fission. The network was incorporated into the microscope control feedback loop to trigger faster imaging during fission; this improved the chance of recording structural intermediates during fission.

Box 3

Practical considerations for deep learning-based denoising

When using neural networks to denoise images, the first decision is whether to use a ‘supervised’ or ‘unsupervised’ approach. Supervised methods require high-quality training data, that is, the collection of matched low signal-to-noise ratio (SNR) and high-SNR image pairs. Ideally, these pairs should be perfectly registered in space and time; thus, training data is often acquired by imaging fixed samples. Although often effective, this method assumes a close correspondence between fixed and live samples, which may not be true in practice. Alternatively, training data may be gathered in live samples, acquiring the paired low-SNR and high-SNR training pairs in rapid succession to avoid motion-induced artefacts in the training data. For 3D applications, one useful approach is to image each focal plane in low-light and high-light conditions before progressing to the next focal plane in the imaged stack, thus ensuring that motion is minimized at each axial position. An alternative approach is to image only high-SNR images and generate corresponding low-SNR training data semi-synthetically by adding artificial noise to high-SNR data from living samples^{11,30}.

If collecting high-SNR ground truth images is impractical or impossible, one can use unsupervised deep learning methods (Fig. 1b), which do not require high-SNR ‘ground truth’ images during training. Instead, these methods assume spatial and/or temporal sample continuity and operate directly on a body of noisy images^{32,118,124}. Another advantage of unsupervised methods is that they can be trained on and applied to the same body of data, removing the possibility that the subcellular structures the network was trained on are different from the ones in the data to be denoised. This circumvents a potential problem associated with supervised methods, which may produce spurious predictions when confronted with structures that are under-represented (or unseen) in the training data.

Each of these strategies may be worth testing, which is increasingly feasible since many methods are open-source and offer tutorials. Nevertheless, trying multiple approaches entails considerable effort, and training a network can take hours — often longer than it takes to acquire the data. Moreover, the expertise may not be accessible to every microscopist or biologist. Generally,

supervised training with high-quality data leads to the best denoising and image restoration performance (Fig. 2). Still, unsupervised denoising may be all that is needed to enable the desired analyses and is thus worth considering as a first step.

Perhaps the greatest caveat when using any deep learning method is that the network output is only a prediction of the ‘ground truth’, and thus caution should be exercised in interpreting such output (Fig. 1d). Furthermore, trained networks must themselves deal with uncertainties, and do so in different ways. Recent denoising approaches can sample multiple denoised ‘interpretations’ of raw input data. These samples are drawn from a previously learned distribution of reasonable data appearances. Most supervised and unsupervised approaches, however, return single outputs, which are generally closer to the ‘average’ of all possible denoised interpretations. While these details are known to method developers, they are often not appreciated by users but may help them to better understand to what extent they can trust and interpret restored images. This underscores the importance of an open discourse and consistent training efforts in this area.

Several related points are worth remembering in the specific context of denoising. First, the performance of any denoising method will decrease in the presence of increasing noise (Fig. 2). It can be useful to assess the SNR, illumination intensity or exposure at which the noise is ‘too much’ and the prediction quality becomes unacceptable, remembering that this will be sample and structure dependent²⁹. Obtaining high-SNR images as ‘sanity checks’ is useful if biological interpretation depends critically on the quality of the denoised output. Second, the degree to which the prediction matches the ground truth depends on the structure, with more faithful restoration of larger structures, and those with higher label density and input SNR. Third, networks tend to generalize poorly when presented with images dissimilar to the data they are trained on (Fig. 1b,c). If quantitative conclusions based on signal intensities are desirable, we advise checking if network predictions preserve linearity²⁹, for example, by comparing region of interest intensities in various locations throughout the raw and restored image data and plotting them against each other¹²⁵.

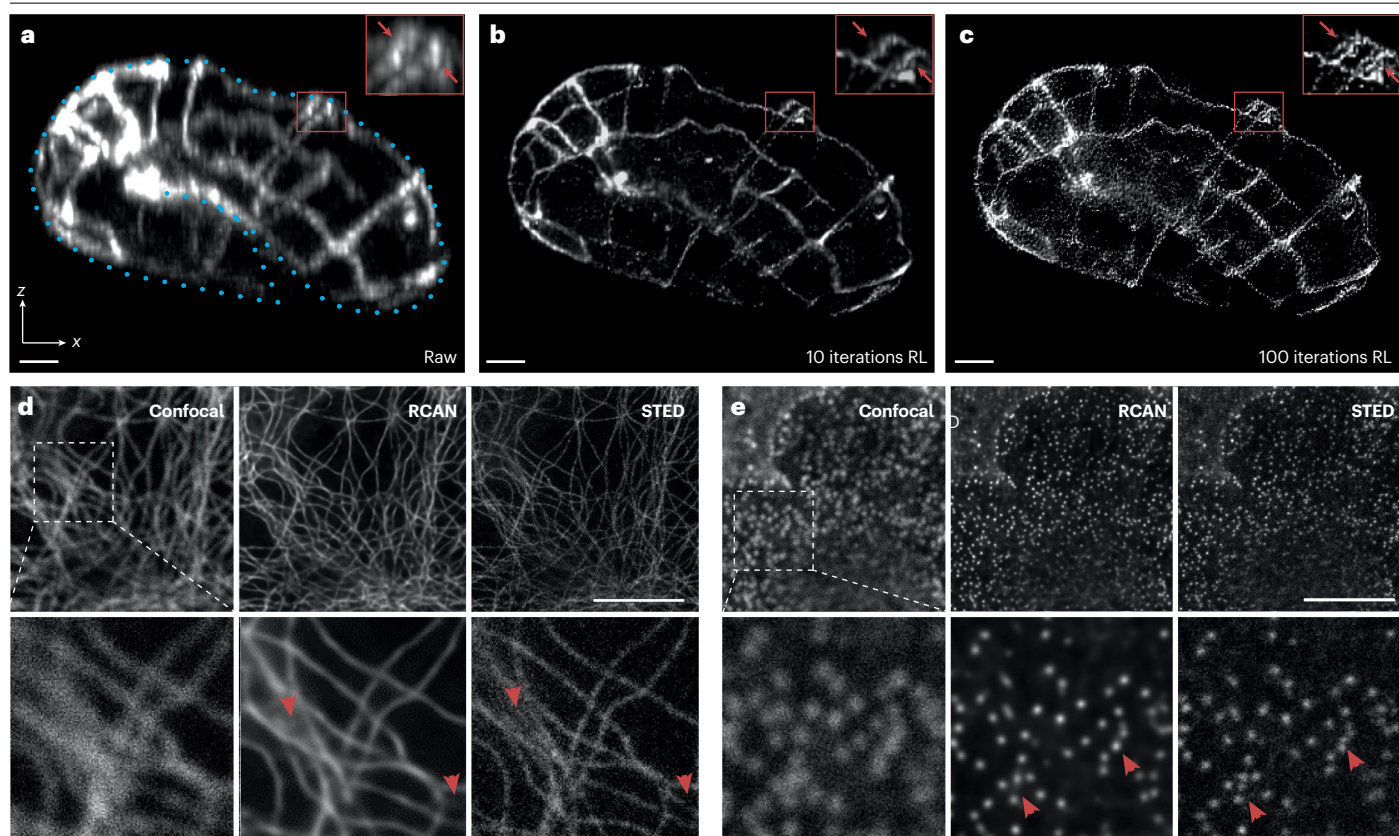


Fig. 3 | Deconvolution and deep learning for image restoration.

a, *Caenorhabditis elegans* embryos expressing an mScarlet junctional marker labelling the interfaces between hypodermal cells were imaged with dual-view light-sheet microscopy. Axial view maximum intensity projection of raw single-view data is shown; embryo boundary outlined with dotted blue lines. Inset shows a higher magnification view of junctional markers in orange rectangular regions, with red arrows highlighting neighbouring cell–cell interfaces. **b**, As in **a**, but after 10 iterations of Richardson–Lucy (RL) deconvolution. Note clear improvement in resolution. **c**, As in **a**, but after 100 iterations of RL. Note amplification of noise and resulting degradation in image quality and spurious structures created by ‘over-sharpening’ interfaces. **d**, Immunolabelled microtubules in fixed mouse embryonic fibroblasts were

imaged with confocal microscopy (left), stimulated emission depletion (STED) microscopy (right) or restored with a residual channel attention network (RCAN) trained to predict STED images from confocal input (middle). Note obvious improvement in resolution with RCAN prediction or STED ground truth but closer inspection (bottom row) reveals that some fine details are lost in the RCAN prediction (red arrows). **e**, As in **d**, but now examining immunolabelled nuclear pore complexes. While RCAN and STED ground truth both reveal more pores than confocal microscopy, RCAN does not accurately predict all pores (red arrows, bottom row). Thus, while both deconvolution and deep learning can enhance the raw data, they are also prone to spurious resolution enhancement and must be interpreted critically and carefully (see also Box 4). Scale bars, 5 μm. Panels **a–c** provided by H.S. Panels **d** and **e** adapted from ref. 29, Springer Nature Limited.

Calcium concentration or pH changes occur rapidly, on the millisecond timescale, during signalling processes. Such changes can be detected by fluorescent sensors, which will display spikes or gradual increases in fluorescence signal. Exocytosis and endocytosis generate calcium spikes, which were detected with widefield microscopy at a high imaging speed (5–10 ms) throughout a large sample region and used in event-triggered STED⁹⁸. The appearance of a spike triggered a shift in imaging modality, from low to high spatial resolution: STED imaging was initiated only in the subcellular region where the calcium spike was detected, saving both time and the rest of the sample from high-intensity exposure.

Multi-colour imaging

Visualizing multiple interacting cellular or tissue components requires tagging them with distinguishable fluorescent markers (fluorophores), which can either be fluorescent dyes or fluorescent proteins. The

engineering and subcellular targeting of fluorescent dyes has a long history, and soon after the first fluorescent proteins were cloned⁹⁹, the engineering of fluorescent protein variants commenced. Today, thousands of dyes and fluorescent proteins are available for use¹⁰⁰.

Fluorophores selected for concurrent use should be chosen such that their emission spectra overlap as little as possible to avoid bleed-through. A similar consideration also holds for excitation spectra, where the undesired excitation of multiple structures by a single excitation wavelength is referred to as ‘crosstalk’. To reduce bleed-through and crosstalk, excitation filters or precise laser excitation wavelengths can be used with emission filters to create a dedicated channel for each fluorophore. FPbase¹⁰⁰ is an excellent open and community-editable resource for designing experiments and enables the selection of specific fluorophores in combination with commercially available excitation sources and filters to reduce bleed-through and crosstalk.

Even with dedicated setups that are carefully optimized for a particular fluorophore combination, it is uncommon to see more than two structures being imaged simultaneously in living specimens. Emission wavelengths range between 400 and 800 nm, and the emission spectral profile for most fluorophores typically spans a band between 50 and 150 nm in width. Thus, on top of increased imaging times and overall light exposure to the sample, with more than three colours, the broad emission and excitation spectra make it increasingly difficult to avoid crosstalk and bleed-through.

The main computational approach for increasing the number of spectral channels available for imaging is spectral unmixing. Instead of imaging multiple fluorescent channels sequentially, a spectrum of intensity versus emitted wavelength is recorded for each detection pixel. The spectrum is used to compute the contribution of each fluorophore to the intensity of each pixel, thereby estimating the proportion of each fluorophore in each pixel. In contrast to non-spectral imaging, where photons of all wavelengths fall on a single detector surface,

a spectral detector typically has multiple separate detection areas that receive different bands of the emitted wavelength. This allows a discretized spectrum to be recorded for each pixel. Another set of methods, based on machine learning inference from label-free images, represents a developing area of research^{101,102}.

Linear unmixing

In the absence of noise, estimating the relative contribution of each fluorescent marker is possible when the number of spectral channels (detected wavelength bands) is at least as large as the number of emitting dyes or fluorescent proteins. Mathematically, this is equivalent to solving a linear system of n equations (which satisfy the constraint that the sum of all individual emissions at each band is equal to the measured total value) with n unknowns (that is, total emission per fluorescent marker) – this approach is known as linear unmixing. For linear unmixing to work, the reference spectra of all fluorescent markers contained in the sample are needed. This is achieved by measuring

Box 4

Practical considerations when using computation to improve spatial resolution

When using deconvolution, one caveat is that algorithms generally assume the point spread function (PSF) of a microscope is spatially invariant, meaning a single blurring function accurately describes the blurring at all locations in the image volume. However, in most microscopes and for most samples, the blurring is spatially variant, particularly as a function of depth due to optical aberrations, or in specialized cases, where the PSF varies by design across the field of view¹²⁶. Accounting for this variation can lead to better deconvolution but is computationally taxing¹²⁷, although a recent deep learning-based implementation¹²⁸ describes an orders-of-magnitude improvement in speed. Another practicality to keep in mind is that the iterative nature of deconvolution can make even the relatively simple deconvolution algorithm (such as the Richardson–Lucy algorithm) time-consuming to execute, so that processing times significantly outweigh data acquisition times, particularly for large datasets. Deciding when to stop the iterative deconvolution process is another challenge, with more iterations improving the image (at the expense of additional computational overhead), but too many iterations leading to noise amplification or unrealistic ‘over-sharpening’ of structures (Fig. 3a–c). Variants of Richardson–Lucy or deep learning approaches designed to mimic deconvolution can considerably shorten this computational overhead or bypass the stopping criterion^{59,129}.

When using deep learning to deblur data, as for denoising applications (Box 3), a major requirement that can limit the use of these methods is acquiring high-quality training data. Acquiring low-resolution and high-resolution image pairs on the same microscope is preferred since it allows easier and more accurate registration between pairs but may be difficult in practice. In such difficult cases, high-resolution data can be computationally degraded to yield semi-synthetic low-resolution data, with high accuracy if

the PSF and noise of the low-resolution data can be estimated^{11,29,30}. In some cases of especially simple image content, the network may be trained on entirely synthetic ground truth that has been blurred and degraded to resemble real biological structures; this approach was used to deblur images of microtubules and secretory granules in living cells¹¹.

A key challenge is assessing the degree to which the deep learning prediction can be trusted. Simulations and experiments indicate that predictions degrade in the presence of increasing noise in the input data and as the degree of resolution enhancement increases, with increasingly obvious deterioration for networks trained to achieve more than twofold resolution enhancement over the raw data^{29,32,125} (Fig. 3d,e). Perhaps the most prudent advice is — as for any imaging experiment — to perform controls, ideally validating the degree of resolution enhancement with other methods such as traditional super-resolution microscopy.

In the future, better reference datasets should enable more comprehensive comparisons across different tools, making it easier for biologists to determine which of the rapidly growing ‘zoo’ of methods can best address a given problem. Still, it is important that users have realistic expectations about what artificial intelligence models can and cannot predict so that their work can remain rigorous and reproducible. For example, artificial neural networks cannot fully recover fine details of structures in diffraction-limited microscopy since information at those spatial scales is lost during image formation. At best, artificial neural networks can make predictions about what such structures might look like based on the raw input image and prior information learned from the training data¹¹. The more stereotyped the structure is and the more similar it is to the training data, the better the predictions are likely to be (Fig. 1c).

Review article

Glossary

Aberrations

Distortions in images generated by an optical system due to deviations in the properties of real optical components, such as lenses, mirrors and filters, as compared with theoretical models or due to refractive index variations in the sample.

Artificial neural network

(ANN). A computational model composed of interconnected nodes and layers, designed to loosely mimic the structure and function of the brain.

Binning

The denoising process of combining data from adjacent pixels in an image, which results in fewer pixels.

Bleed-through

Overlap in the emission spectra of two distinct fluorophores, leading to detection of both at the same wavelength.

Centroid

The centre position of an object, corresponding to the weighted mean of pixel intensity values.

Continuity

Property of an object consisting of containing no resolved gaps in space (spatial continuity) or time (temporal continuity).

Crosstalk

Undesired mixing of signals. For example, overlap in the excitation spectra of two distinct fluorophores, leading to excitation of both by the same wavelength of light. Or, in multi-focal microscopy, fluorescence from one excitation spot contributing to the signal of neighbouring regions.

Deconvolution

Since an image is blurred by the convolution of the fluorescently labelled object with the point spread function of the microscope, this image processing method attempts to computationally reverse this effect.

Deep learning

A class of machine learning algorithms based on artificial neural networks containing multiple data processing layers.

Depletion doughnut

A doughnut-shaped illumination light used to turn off the fluorescence in the periphery of the focal spot.

Downsampling

Reducing the sampling rate, for example, spatially or temporally.

Dwell time

The time a focused laser beam is applied to each location in the specimen being imaged.

Fluorescence lifetime

The time a fluorophore spends in the excited state before emitting a photon and returning to the ground state.

Gaussian readout noise

Noise that follows a Gaussian distribution and is independent of pixel intensity values, for example, noise generated by a camera chip when it converts charge into voltage.

Ground truth

The target of a deep learning model, for example, a label against which the predictions of a model are compared during training.

Hallucinations

Neural network outputs that look plausible but have no basis in the input data.

Lattice light-sheet

Light-sheet generated by scanning a 2D lattice of structured light known as Bessel beams.

Light-sheet microscopy

Method in which a thin slice of a specimen is illuminated perpendicular to the imaging orientation.

Linearity

The property of two quantities (for example, intensities) being linearly

proportional, such that their values are related by a multiplicative constant.

Low-pass filter

An operation that passes frequencies below a cut-off value, which corresponds to retaining lower-resolution features in an image.

Mean absolute error

(MAE). The mean of the absolute value of the difference between measured and predicted values, for example, ground truth pixel intensity values and those output by a network. Used as a metric of how well a model captures the data.

Mean squared error

(MSE). The mean squared difference between measured and predicted values, for example, ground truth pixel intensity values and those output by a network. Used as a metric of how well a model captures the data.

Median filtering

An operation that replaces the intensity value in a pixel with the median value of its neighbours.

Multiphoton microscopy

Method in which multiple photons must be simultaneously absorbed by a single fluorophore to bring it into its excited state.

Mutual information

A measure of the extent to which two quantities depend on one another, related to how precisely one quantity can be predicted based on the value of the other.

Nyquist–Shannon sampling theorem

Principle that defines the maximum spacing between measurements that will be sufficient to determine a given frequency component within a signal; for example, to resolve dynamics at a timescale of T seconds, the time between images should be less than T/2.

Peak signal-to-noise ratio

(PSNR). The ratio between the squared maximum possible signal in an image

and the mean squared error. This is reported in units of decibels, so the logarithm of the ratio is taken and multiplied by 10. Used as a metric of how well a model captures the data.

Photon budget

Fluorescence signal detected from an object of interest during an experiment, typically finite due to photobleaching.

Point spread function

The intensity distribution of a point-like source when imaged through a microscope.

Poisson noise

Noise (that is, shot noise) that follows a Poisson distribution, for example, arising from measuring photons because they are discrete particles.

Pyramid of frustration

Concept illustrating the tradeoffs in fluorescence microscopy, where each axis defines one measurement property such as signal-to-noise ratio or spatial or temporal resolution. The fixed photon budget implies that improving along one dimension leads to degradation along another.

Reference datasets

Data used within a field to compare the performance of algorithms, in benchmarking comparisons.

Reversible saturable optical fluorescence transitions

(RESOLFT). A super-resolution technique suitable for live-cell imaging and based on reversibly switching fluorescent probes and patterned illumination.

Sampling

Recording a signal in a discontinuous manner, at specific locations or times.

Signal-to-noise ratio

(SNR). The ratio between signal and noise that can be estimated on a per-pixel basis as the mean intensity value divided by the standard deviation of the intensity.

Review article

Glossary (continued)

Single-molecule localization microscopy

(SMLM). A class of super-resolution microscopy techniques based on imaging single molecules whose signals have been isolated, then combining their sub-pixel locations to form a composite image.

Spatial frequencies

Just as a function can be decomposed into a sum of sines and cosines (compared with Fourier transform), an image can be decomposed into a sum of waves with different spatial frequencies. These represent the image at different resolution levels, with higher spatial frequencies describing finer image details and lower spatial frequencies describing coarser details.

Spatial resolution

The smallest distance at which two features can be distinguished.

Spectrum

Response of a fluorophore as a function of wavelength of light. The excitation spectrum reflects the capacity of light

absorbed at different wavelengths to generate fluorescence of a particular wavelength, while the emission spectrum reflects the emission of light at different wavelengths following excitation at a particular wavelength.

Spinning disk confocal microscopy

Method in which an array of focused excitation laser beams is produced by an array of microlenses on a disk that spins to scan the specimen. Out-of-focus emission light is rejected by a confocal array of pinholes.

Statistical distance

An objective score that summarizes statistical differences between two objects, for example, between a prediction and the training set in machine learning. Possibilities include ‘total variational distance’ and ‘Kullback–Liebler divergence’.

Stimulated emission depletion (STED) microscopy

A super-resolution technique based on patterned

illumination, typically doughnut shaped, which is used to deplete the fluorescence of commonly used fluorescent probes.

Structural similarity index measure

(SSIM). A measure of how similar two images are based on distortions that humans tend to perceive: the weighted product of luminance (average brightness), contrast (standard deviation of pixel intensity values) and structure (cross-covariance).

Structured illumination microscopy

(SIM). A class of super-resolution microscopy techniques that use patterned excitation light combined with optical or digital image processing to recover information below the diffraction limit.

Super-resolution

Imaging techniques that achieve spatial resolutions surpassing the diffraction limit of light.

Synthetic data

Data generated computationally using a model. Can be combined with real data to create semi-synthetic data.

Temporal resolution

The time between consecutive images of the same part of the specimen.

Total internal reflection fluorescence

Method in which a specimen is illuminated at the coverslip–media interface by an evanescent field generated by a laser at an incident angle sufficient to cause total internal reflection.

Training data

Data used to train a machine learning algorithm to make predictions based on supervised learning. The quality and quantity of training data are key determinants of the performance of artificial neural networks.

each spectrum individually or by manually identifying regions in an acquired image that contain only one of the fluorescent markers. Automated component extraction procedures exist commercially and can potentially help to avoid this manual calibration step.

In any experiment, the acquired data will be subject to noise, for example, Poisson shot noise and Gaussian readout noise. The presence of noise poses problems for linear unmixing by making multiple solutions plausible (that is, the unmixing result is no longer unique). Hence, the contributions from the different fluorophores cannot be correctly assigned. Intensity saturation, sample photobleaching, autofluorescence or other undesired sources of light being imaged (for example, room lights) also degrade the performance of linear unmixing. In the next sections, we will discuss unmixing strategies that better address these issues.

Blind unmixing

Blind unmixing enables fluorophore separation without prior knowledge of emission spectra and a minimal number of detection channels, typically less than the number of fluorophores to be unmixed. One such algorithm, LUMoS (learning unsupervised means of spectra)¹⁰³, learns the relationship between pixels in the raw imaging data and intensity patterns and uses this information to re-classify each pixel into a fluorophore group. This unsupervised approach was applied to two-photon microscopy data of cultured cells and separated up to six channels using only four detectors, which helped to reduce

hardware complexity. The accuracy of the separation algorithm was also tested under challenging conditions such as low SNR, significant autofluorescence and structures of different sizes.

Another blind unmixing approach is PICASSO (Process of Ultra-Multiplexed Imaging of Biomolecules via the Unmixing of the Signals of Spectrally Overlapping Fluorophores)¹⁰⁴. This method is based on the concept that, when the emission spectra from multiple fluorophores mix together, the mutual information between detection channels increases. Thus, the unmixed information containing fluorophore abundances in each part of the image can be retrieved by iteratively minimizing the mutual information between detection channels. For this strategy to work, it is necessary to record images in at least as many distinct channels as the number of fluorophore species – and for each fluorophore species to have one spectral channel in which it appears brighter than it does in the other channels. This tool was used to separate five spectrally overlapping fluorophores excited with a single laser line and up to fifteen fluorophores with the use of multiple excitation laser lines and was experimentally validated with 3D images of antibody-stained mouse brain slices.

Unmixing spectral and fluorescence lifetime signals

Fluorescence lifetime refers to the kinetics of fluorescence emission and is a property intrinsic to fluorophores, which can be used to deduce molecular identity without relying on excitation or emission spectra. Linear and blind unmixing strategies can also be applied to fluorescence

lifetime imaging microscopy (FLIM) signals. Recording FLIM data can be slow since many photons are needed to reconstruct the fluorescence lifetime decay. Recent developments in electronics and detectors improved the acquisition speed, enabling simultaneous lifetime and spectral detection. Data processing is not trivial due to the size of the raw data, which contains both spectral and temporal information on each pixel of the image.

The Phasor approach¹⁰⁵ was developed to simplify data visualization and reduce post-processing time. It provides a graphical overview as a Phasor plot: a 2D histogram of the processes affecting the fluorescence lifetime decay occurring at each pixel. Long-lifetime and short-lifetime decays are located at different positions, and single and multi-exponential decays are also separated. The Phasor approach is commercially available and can be used to record multiple molecular species at the same time, labelled with fluorophores with different spectra or lifetimes. Phasors have also been used to improve the quality of super-resolution STED data by efficiently separating the fluorescence signal carrying low-resolution information¹⁰⁶.

Blind approaches, such as Phasor S-FLIM, can unmix images with a sufficiently large number of FLIM photons (tens to hundreds per pixel)¹⁰⁷. Additional approaches based on deep learning have also been applied to multispectral fluorescence lifetime imaging data. UNMIX-ME (unmix multiple emissions)¹⁰⁸ is capable of quantitative fluorophore unmixing by simultaneously using both spectral and temporal signatures. While these algorithms have shown great potential in separating multiple molecular species, collecting FLIM data requires specialized detectors as does spectral imaging. Microscopes equipped with such spectral and lifetime detectors have become more common in core facilities, and the development of these kinds of computational methods for interpreting the data they produce will likely lead to increased insight into complex multi-molecular processes.

Discussion and outlook

We have highlighted recent developments in computational approaches which we find to be most promising in terms of their immediate or near-term potential for improving live-cell imaging. Although we divided techniques according to their improvement to the SNR, spatial resolution, temporal resolution and multichannel imaging, some of these distinctions are practically convenient rather than fundamental. This is because all axes are linked to photon budget and light exposure and, in that sense, gains along one axis can be traded for gains along another. For instance, an acquisition that uses denoising to cope with lower SNR can image faster, or with higher resolution, or in more colour channels. Alternatively, it may be possible to improve all these parameters to a lesser extent. The optimal compromise will depend on the scientific question under investigation.

Computational approaches, especially those based on machine learning, represent a vibrant area of research whose current limitations are also important to understand¹⁰⁹. We expect that future developments will improve the specific tools mentioned here. In that regard, it is important to place into context significant improvements that users should strive to adopt versus marginal gains that could be important in special cases. One may draw parallels here with the development of super-resolution localization microscopy, in which algorithms and software packages proliferated during a flurry of activity. In that case, a valuable resource for the community was a benchmarking challenge that allowed developers and users to more directly compare the performance⁵⁷. A similar resource would be welcome in each of the application spaces described here. In addition,

no general-purpose tool currently exists for assessing uncertainty in predictions that a neural network generates. Such a tool would be enormously beneficial to a biologist end-user, allowing them to assess when predictions should not be trusted and thus excluded from downstream analyses.

Most machine learning-based approaches are ‘data driven’ and do not rely on scientific principles, which can be an advantage. However, this may also limit their performance – humans remain better able to generalize and learn from much less data. We are aided by centuries of science, which have relied on model building to ‘make sense’ of patterns, whether physics-based, mathematical or the more heuristic, graphical schema often found in biology. In the case of microscopy, optical physics and engineering are reliably used to quantitatively model and interpret biological imaging experiments. In the future, these priors could be used to validate and further improve existing neural network methods or to reduce artefacts to overcome some of the current issues in computational microscopy.

Multi-colour imaging and imaging at depth are areas that we think will see exciting growth in the coming years. It is still difficult to routinely image with more than a few colours, and it is still hard to image deep inside samples with the clarity that we can obtain when imaging at the coverslip. Given the difficulties associated with pure hardware solutions, we suspect computation will have an important part to play in these efforts. So far, purely computational methods are less demonstrated to go directly from low temporal resolution to high temporal resolution or small imaging volumes to large ones. These contexts are especially challenging for machine learning approaches since ground truth data is difficult to obtain¹¹⁰. Moreover, many dynamic processes in biology are intermittent, non-deterministic and take place across multiple timescales – thus, networks that try to predict the dynamics between two collected images are unlikely to be reliable. Similarly, for volumetric imaging, inferring content in unseen planes assumes continuity but structures may be discontinuous and contain information across multiple length scales. Thus, we expect that combining computation and hardware will offer a promising approach to these challenges.

We anticipate that integration between computation and microscope hardware will continue to develop to enable more informative automated data acquisitions. Early examples of smart microscopy, in which data is used in real time to adapt an acquisition, have already demonstrated that ANNs can detect contextually rich biological events and feed them back to the microscope as a cue to change the measurement. By prioritizing SNR, temporal and spatial resolution, or multi-colour imaging for events of interest or optimizing image quality in real time, it is possible to more efficiently capture the data that is most relevant to test hypotheses. This offers a way to repurpose machine learning tools developed for segmentation or other image-processing tasks to improve the data at its source. Extending beyond photon budget limitations, the fields of systems biology and neuroscience have made significant inroads into using optogenetic control to dissect genetic¹¹¹ or neuronal¹¹² circuits using real-time activation and feedback loops. These methods, combined, may eventually allow concepts used to derive natural physical laws algorithmically from data¹¹³ to be extended to biological systems by determining which experiments should be done next to best constrain a model.

The complexity of an end-to-end microscopy experiment (from sample preparation to acquisition to analysis and interpretation) has increased enormously in recent years as biological samples are prepared to better resemble native specimens, microscopes leverage

advances in optics and automation, and analyses attempt to recover as much information as possible. This can present daunting challenges for researchers who lack access to advanced infrastructures. A dream solution would be enhanced collaboration between microscope users and hardware and software developers. As examples, Janelia's Advanced Imaging Center and the Eurobioimaging infrastructure offer access to imaging technologies, training and support. While these efforts have outsized impact by allowing access to a broad range of users independent of their institutional affiliations, more is needed to encourage exchanges in the area of computation¹¹⁴, for example, through consortia like AI4Life as well as resources like Micro-manager¹¹⁵ and the BioImage Model Zoo¹¹⁶.

Published online: 20 February 2024

References

1. Ducret, A., Quardokus, E. M. & Brun, Y. V. MicrobeJ, a tool for high throughput bacterial cell detection and quantitative analysis. *Nat. Microbiol.* **1**, 16077 (2016).
2. Levet, F. et al. SR-Tesseler: a method to segment and quantify localization-based super-resolution microscopy data. *Nat. Methods* **12**, 1065–1071 (2015).
3. Rizk, A. et al. Segmentation and quantification of subcellular structures in fluorescence microscopy images using Squash. *Nat. Protoc.* **9**, 586–596 (2014).
4. Ulman, V. et al. An objective comparison of cell-tracking algorithms. *Nat. Methods* **14**, 1141–1152 (2017).
5. Axelrod, D., Koppel, D. E., Schlessinger, J., Elson, E. & Webb, W. W. Mobility measurement by analysis of fluorescence photobleaching recovery kinetics. *Biophys. J.* **16**, 1055–1069 (1976).
6. Elson, E. L. & Magde, D. Fluorescence correlation spectroscopy. I. Conceptual basis and theory. *Biopolymers* **13**, 1–27 (1974).
7. Gahlmann, A. & Moerner, W. E. Exploring bacterial cell biology with single-molecule tracking and super-resolution imaging. *Nat. Rev. Microbiol.* **12**, 9–22 (2014).
8. Saxton, M. J. & Jacobson, K. Single-particle tracking: applications to membrane dynamics. *Annu. Rev. Biophys. Biomol. Struct.* **26**, 373–399 (1997).
9. Moen, E. et al. Deep learning for cellular image analysis. *Nat. Methods* **16**, 1233–1246 (2019).
10. Van Valen, D. A. et al. Deep learning automates the quantitative analysis of individual cells in live-cell imaging experiments. *PLoS Comput. Biol.* **12**, e1005177 (2016).
11. Weigert, M. et al. Content-aware image restoration: pushing the limits of fluorescence microscopy. *Nat. Methods* **15**, 1090–1097 (2018).
12. Lajisse, P. P., Alghamdi, R. A., Tomancak, P., Reynaud, E. G. & Shroff, H. Assessing phototoxicity in live fluorescence imaging. *Nat. Methods* **14**, 657–661 (2017).
13. Grimm, J. B. et al. A general method to improve fluorophores for live-cell and single-molecule microscopy. *Nat. Methods* **12**, 244–250 (2015).
14. Lukinavičius, G. et al. A near-infrared fluorophore for live-cell super-resolution microscopy of cellular proteins. *Nat. Chem.* **5**, 132–139 (2013).
15. Shaner, N. C. et al. Improving the photostability of bright monomeric orange and red fluorescent proteins. *Nat. Methods* **5**, 545–551 (2008).
16. Gustafsson, M. G. L. et al. Three-dimensional resolution doubling in wide-field fluorescence microscopy by structured illumination. *Biophys. J.* **94**, 4957–4970 (2008).
17. Hell, S. W. Far-field optical nanoscopy. *Science* **316**, 1153–1158 (2007).
18. Betzig, E. et al. Imaging intracellular fluorescent proteins at nanometer resolution. *Science* **313**, 1642–1645 (2006).
19. Rust, M. J., Bates, M. & Zhuang, X. Sub-diffraction-limit imaging by stochastic optical reconstruction microscopy (STORM). *Nat. Methods* **3**, 793–795 (2006).
20. Denk, W., Strickler, J. H. & Webb, W. W. Two-photon laser scanning fluorescence microscopy. *Science* **248**, 73–76 (1990).
21. Huisken, J., Swoger, J., Del Bene, F., Wittbrodt, J. & Stelzer, E. H. K. Optical sectioning deep inside live embryos by selective plane illumination microscopy. *Science* **305**, 1007–1009 (2004).
22. Möckl, L., Roy, A. R., Petrov, P. N. & Moerner, W. E. Accurate and rapid background estimation in single-molecule localization microscopy using the deep neural network BGNet. *Proc. Natl. Acad. Sci. USA* **117**, 60–67 (2020).
23. Schindelin, J. et al. Fiji: an open-source platform for biological-image analysis. *Nat. Methods* **9**, 676–682 (2012).
24. Huang, T. S., Yang, G. J. & Tang, G. Y. A fast two-dimensional median filtering algorithm. *IEEE Trans. Signal. Process.* **27**, 13–18 (1979).
25. Strong, D. & Chan, T. Edge-preserving and scale-dependent properties of total variation regularization. *Inverse Problems* **19**, S165–S187 (2003).
26. Buades, A., Coll, B. & Morel, J. M. A non-local algorithm for image denoising. *IEEE Computer Society Conference on Computer Vision and Pattern Recognition (CVPR'05)*, 60–65 (2005).
27. Huang, X. et al. Fast, long-term, super-resolution imaging with Hessian structured illumination microscopy. *Nat. Biotechnol.* **36**, 451–459 (2018).
28. Lecun, Y., Bengio, Y. & Hinton, G. Deep learning. *Nature* **521**, 436–444 (2015).
29. Chen, J. et al. Three-dimensional residual channel attention networks denoise and sharpen fluorescence microscopy image volumes. *Nat. Methods* **18**, 678–687 (2021).
30. Fang, L. et al. Deep learning-based point-scanning super-resolution imaging. *Nat. Methods* **18**, 406–416 (2021).
31. Qiao, C. et al. Evaluation and development of deep neural networks for image super-resolution in optical microscopy. *Nat. Methods* **18**, 194–202 (2021).
32. Qiao, C. et al. Rationalized deep learning super-resolution microscopy for sustained live imaging of rapid subcellular processes. *Nat. Biotechnol.* **41**, 367–377 (2023).
33. Gustafsson, M. G. L. Surpassing the lateral resolution limit by a factor of two using structured illumination microscopy. *J. Microsc.* **198**, 82–87 (2000).
34. Chen, B. C. et al. Lattice light-sheet microscopy: imaging molecules to embryos at high spatiotemporal resolution. *Science* **346**, 1257998 (2014).
35. York, A. G. et al. Instant super-resolution imaging in live cells and embryos via analog image processing. *Nat. Methods* **10**, 1122–1130 (2013).
36. Hoebe, R. A. et al. Controlled light-exposure microscopy reduces photobleaching and phototoxicity in fluorescence live-cell imaging. *Nat. Biotechnol.* **25**, 249–253 (2007).
37. Chu, K. K., Lim, D. & Mertz, J. Enhanced weak-signal sensitivity in two-photon microscopy by adaptive illumination. *Opt. Lett.* **32**, 2846–2848 (2007).
38. Li, B., Wu, C., Wang, M., Charan, K. & Xu, C. An adaptive excitation source for high-speed multiphoton microscopy. *Nat. Methods* **17**, 163–166 (2020).
39. Staudt, T. et al. Far-field optical nanoscopy with reduced number of state transition cycles. *Opt. Express* **19**, 5644–5657 (2011).
40. Chakrava, N., Canton, A. S., Danelon, C., Stallinga, S. & Rieger, B. Adaptive illumination reduces photobleaching in structured illumination microscopy. *Biomed. Opt. Express* **7**, 4263–4274 (2016).
41. Göttfert, F. et al. Strong signal increase in STED fluorescence microscopy by imaging regions of subdiffraction extent. *Proc. Natl. Acad. Sci. USA* **114**, 2125–2130 (2017).
42. Heine, J. et al. Adaptive-illumination STED nanoscopy. *Proc. Natl. Acad. Sci. USA* **114**, 9797–9802 (2017).
43. Dreier, J. et al. Smart scanning for low-illumination and fast RESOLFT nanoscopy in vivo. *Nat. Commun.* **10**, 556 (2019).
44. Vinçon, B., Geisler, C. & Egner, A. Pixel hopping enables fast STED nanoscopy at low light dose. *Opt. Express* **28**, 4516–4528 (2020).
45. Štefko, M., Ottino, B., Douglass, K. M. & Manley, S. Autonomous illumination control for localization microscopy. *Opt. Express* **26**, 30882–30900 (2018).
46. Chiron, L. et al. CyberScoPy: an open-source software for event-based, conditional microscopy. *Sci. Rep.* **12**, 11579 (2022).
47. Almada, P. et al. Automating multimodal microscopy with NanoJ-Fluidics. *Nat. Commun.* **10**, 1223 (2019).
48. Edelstein, A. D. et al. Advanced methods of microscope control using μManager software. *J. Biol. Methods* **1**, e10 (2014).
49. Pinkard, H., Stuurman, N., Corbin, K., Vale, R. & Krummel, M. F. Micro-Magellan: open-source, sample-adaptive, acquisition software for optical microscopy. *Nat. Methods* **13**, 807–809 (2016).
50. Fox, Z. R. et al. Enabling reactive microscopy with MicroMator. *Nat. Commun.* **13**, 2199 (2022).
51. Casas Moreno, X. et al. An open-source microscopy framework for simultaneous control of image acquisition, reconstruction, and analysis. *HardwareX* **13**, e00400 (2023).
52. Schermelleh, L. et al. Super-resolution microscopy demystified. *Nat. Cell Biol.* **21**, 72–84 (2019).
53. Wu, Y. & Shroff, H. Multiscale fluorescence imaging of living samples. *Histochem. Cell Biol.* **158**, 301–323 (2022).
54. Sarder, P. & Nehorai, A. Deconvolution methods for 3-D fluorescence microscopy images. *IEEE Signal. Process. Mag.* **23**, 32–45 (2006).
55. Lucy, L. B. An iterative technique for the rectification of observed distributions. *Astron. J.* **79**, 745–754 (1974).
56. Richardson, W. H. Bayesian-based iterative method of image restoration. *J. Opt. Soc. Am.* **62**, 55–59 (1972).
57. Sage, D. et al. DeconvolutionLab2: an open-source software for deconvolution microscopy. *Methods* **115**, 28–41 (2017).
58. Zhao, W. et al. Sparse deconvolution improves the resolution of live-cell super-resolution fluorescence microscopy. *Nat. Biotechnol.* **40**, 606–617 (2022).
59. Li, Y. et al. Incorporating the image formation process into deep learning improves network performance. *Nat. Methods* **19**, 1427–1437 (2022).
60. Chherti, R. K. et al. Whole-animal functional and developmental imaging with isotropic spatial resolution. *Nat. Methods* **12**, 1171–1178 (2015).
61. Wu, Y. et al. Spatially isotropic four-dimensional imaging with dual-view plane illumination microscopy. *Nat. Biotechnol.* **31**, 1032–1038 (2013).
62. Wu, Y. et al. Multiview confocal super-resolution microscopy. *Nature* **600**, 279–284 (2021).
63. Ingaramo, M. et al. Richardson-Lucy deconvolution as a general tool for combining images with complementary strengths. *ChemPhysChem* **15**, 794–800 (2014).
64. Kazemipour, A. et al. Kilohertz frame-rate two-photon tomography. *Nat. Methods* **16**, 778–786 (2019).
65. Wang, H. et al. Deep learning enables cross-modality super-resolution in fluorescence microscopy. *Nat. Methods* **16**, 103–110 (2019).

66. Li, X. et al. Three-dimensional structured illumination microscopy with enhanced axial resolution. *Nat. Biotechnol.* **41**, 1307–1319 (2023).
67. Weigert, M., Royer, L., Jug, F. & Myers, G. Isotropic reconstruction of 3D fluorescence microscopy images using convolutional neural networks. Preprint at <https://doi.org/10.48550/arXiv.1704.01510> (2017).
68. Hampson, K. M. et al. Adaptive optics for high-resolution imaging. *Nat. Rev. Methods Prim.* **1**, 68 (2021).
69. Ji, N. Adaptive optical fluorescence microscopy. *Nat. Methods* **14**, 374–380 (2017).
70. Wang, K. et al. Rapid adaptive optical recovery of optimal resolution over large volumes. *Nat. Methods* **11**, 625–628 (2014).
71. Liu, T. L. et al. Observing the cell in its native state: imaging subcellular dynamics in multicellular organisms. *Science* **360**, eaao1392 (2018).
72. Rodríguez, C. et al. An adaptive optics module for deep tissue multiphoton imaging *in vivo*. *Nat. Methods* **18**, 1259–1264 (2021).
73. Streich, L. et al. High-resolution structural and functional deep brain imaging using adaptive optics three-photon microscopy. *Nat. Methods* **18**, 1253–1258 (2021).
74. Lin, R., Kipreos, E. T., Zhu, J., Khang, C. H. & Kner, P. Subcellular three-dimensional imaging deep through multicellular thick samples by structured illumination microscopy and adaptive optics. *Nat. Commun.* **12**, 3148 (2021).
75. Zheng, W. et al. Adaptive optics improves multiphoton super-resolution imaging. *Nat. Methods* **14**, 869–872 (2017).
76. Saha, D. et al. Practical sensorless aberration estimation for 3D microscopy with deep learning. *Opt. Express* **28**, 29044–29053 (2020).
77. Vinogradova, K. & Myers, E.W. Estimation of optical aberrations in 3D microscopic bioimages. *7th International Conference on Frontiers of Signal Processing, ICSP*, 97–103 (2022).
78. Feng, B. Y. et al. NeuWS: neural wavefront shaping for guidestar-free imaging through static and dynamic scattering media. *Sci. Adv.* **9**, eadg4671 (2023).
79. Balzaretti, F. et al. Nanometer resolution imaging and tracking of fluorescent molecules with minimal photon fluxes. *Science* **355**, 606–612 (2017).
80. Deguchi, T. et al. Direct observation of motor protein stepping in living cells using MINFLUX. *Science* **379**, 1010–1015 (2023).
81. Wolff, J. O. et al. MINFLUX dissects the unimpeded walking of kinesin-1. *Science* **379**, 1004–1010 (2023).
82. Royer, L. A. et al. Adaptive light-sheet microscopy for long-term, high-resolution imaging in living organisms. *Nat. Biotechnol.* **34**, 1267–1278 (2016).
83. Pinkard, H. et al. Learned adaptive multiphoton illumination microscopy for large-scale immune response imaging. *Nat. Commun.* **12**, 1916 (2021).
84. Durand, A. et al. A machine learning approach for online automated optimization of super-resolution optical microscopy. *Nat. Commun.* **9**, 5247 (2018).
85. Sheppard, C. J. R. Super-resolution in confocal imaging. *Optik* **80**, 53–54 (1988).
86. Müller, C. B. & Enderlein, J. Image scanning microscopy. *Phys. Rev. Lett.* **104**, 74–83 (2010).
87. York, A. G. et al. Resolution doubling in live, multicellular organisms via multifocal structured illumination microscopy. *Nat. Methods* **9**, 749–754 (2012).
88. Schulz, O. et al. Resolution doubling in fluorescence microscopy with confocal spinning-disk image scanning microscopy. *Proc. Natl Acad. Sci. USA* **110**, 21000–21005 (2013).
89. De Luca, G. M. R. et al. Re-scan confocal microscopy: scanning twice for better resolution. *Biomed. Opt. Express* **4**, 2644–2656 (2013).
90. Roth, S., Sheppard, C. J. R., Wicker, K. & Heintzmann, R. Optical photon reassignment microscopy (OPRA). *Opt. Nanoscopy* **2**, 5 (2013).
91. Azuma, T. & Kei, T. Super-resolution spinning-disk confocal microscopy using optical photon reassignment. *Opt. Express* **23**, 15003–15011 (2015).
92. Hofmann, M., Eggeling, C., Jakobs, S. & Hell, S. W. Breaking the diffraction barrier in fluorescence microscopy at low light intensities by using reversibly photoswitchable proteins. *Proc. Natl Acad. Sci. USA* **102**, 17565–17569 (2005).
93. Chmyrov, A. et al. Nanoscopy with more than 100,000 ‘doughnuts’. *Nat. Methods* **10**, 737–740 (2013).
94. Bodén, A. et al. Volumetric live cell imaging with three-dimensional parallelized RESOLFT microscopy. *Nat. Biotechnol.* **39**, 609–618 (2021).
95. Lelek, M. et al. Single-molecule localization microscopy. *Nat. Rev. Methods Prim.* **1**, 39 (2021).
96. Speiser, A. et al. Deep learning enables fast and dense single-molecule localization with high accuracy. *Nat. Methods* **18**, 1082–1090 (2021).
97. Mahecic, D. et al. Event-driven acquisition for content-enriched microscopy. *Nat. Methods* **19**, 1262–1267 (2022).
98. Alvelid, J., Damenti, M., Sgattoni, C. & Testa, I. Event-triggered STED imaging. *Nat. Methods* **19**, 1268–1275 (2022).
99. Tsien, R. Y. The green fluorescent protein. *Annu. Rev. Biochem.* **67**, 509–544 (1998).
100. Lambert, T. J. FPbase: a community-editable fluorescent protein database. *Nat. Methods* **16**, 277–278 (2019).
101. Cheng, S. et al. Single-cell cytometry via multiplexed fluorescence prediction by label-free reflectance microscopy. *Sci. Adv.* **7**, eabe0431 (2021).
102. Christiansen, E. M. et al. In silico labeling: predicting fluorescent labels in unlabeled images. *Cell* **173**, 792–803.e19 (2018).
103. McRae, T. D., Oleksyn, D., Miller, J. & Gao, Y.-R. Robust blind spectral unmixing for fluorescence microscopy using unsupervised learning. *PLoS One* **14**, e0225410 (2019).
104. Seo, J. et al. PICASSO allows ultra-multiplexed fluorescence imaging of spatially overlapping proteins without reference spectra measurements. *Nat. Commun.* **13**, 2475 (2022).
105. Digman, M. A., Caiolfa, V. R., Zamai, M. & Gratton, E. The phasor approach to fluorescence lifetime imaging analysis. *Biophys. J.* **94**, L14–L16 (2008).
106. Lanzanò, L. et al. Encoding and decoding spatio-temporal information for super-resolution microscopy. *Nat. Commun.* **6**, 6701 (2015).
107. Scipioni, L., Rossetta, A., Tedeschi, G. & Gratton, E. Phasor S-FLIM: a new paradigm for fast and robust spectral fluorescence lifetime imaging. *Nat. Methods* **18**, 542–550 (2021).
108. Smith, J. T., Ochoa, M. & Intes, X. UNMIX-ME: spectral and lifetime fluorescence unmixing via deep learning. *Biomed. Opt. Express* **11**, 3857–3874 (2020).
109. Belthangady, C. & Royer, L. A. Applications, promises, and pitfalls of deep learning for fluorescence image reconstruction. *Nat. Methods* **16**, 1215–1225 (2019).
110. Saguy, A. et al. DBLink: dynamic localization microscopy in super spatiotemporal resolution via deep learning. *Nat. Methods* **20**, 1939–1948 (2023).
111. Milius-Argeitis, A. et al. In silico feedback for *in vivo* regulation of a gene expression circuit. *Nat. Biotechnol.* **29**, 1114–1116 (2011).
112. Emiliiani, V., Cohen, A. E., Deisseroth, K. & Häusser, M. All-optical interrogation of neural circuits. *J. Neurosci.* **35**, 13917–13926 (2015).
113. Schmidt, M. & Lipson, H. Distilling free-form natural laws from experimental data. *Science* **324**, 81–85 (2009).
114. Colón-Ramos, D. A., La Rivière, P., Shroff, H. & Oldenbourg, R. Transforming the development and dissemination of cutting-edge microscopy and computation. *Nat. Methods* **16**, 667–669 (2019).
115. Conrad, C. et al. Micropilot: automation of fluorescence microscopy-based imaging for systems biology. *Nat. Methods* **8**, 246–249 (2011).
116. Ouyang, W. et al. BiolImage model zoo: a community-driven resource for accessible deep learning in bioimage analysis. Preprint at *bioRxiv* <https://doi.org/10.1101/2022.06.07.495102> (2022).
117. Katona, G. et al. Fast two-photon *in vivo* imaging with three-dimensional random-access scanning in large tissue volumes. *Nat. Methods* **9**, 201–208 (2012).
118. Krull, A., Buchholz, T. O. & Jug, F. Noise2void – learning denoising from single noisy images. Preprint at <https://doi.org/10.48550/arXiv.1811.10980> (2019).
119. Ouyang, W., Aristov, A., Lelek, M., Hao, X. & Zimmer, C. Deep learning massively accelerates super-resolution localization microscopy. *Nat. Biotechnol.* **36**, 460–468 (2018).
120. Greener, J. G., Kandathil, S. M., Moffat, L. & Jones, D. T. A guide to machine learning for biologists. *Nat. Rev. Mol. Cell Biol.* **23**, 40–55 (2022).
121. Wang, Z., Bovik, A. C., Sheikh, H. R. & Simoncelli, E. P. Image quality assessment: from error visibility to structural similarity. *IEEE Trans. Image Process.* **13**, 600–612 (2004).
122. Wang, Z., Simoncelli, E.P. & Bovik, A.C. Multiscale structural similarity for image quality assessment. In *37th Asilomar Conference on Signals, Systems & Computers, 2003 Vol. 2*, 1398–1402 (2003).
123. Zhang, R., Isola, P., Efros, A.A., Shechtman, E. & Wang, O. The unreasonable effectiveness of deep features as a perceptual metric. In *2018 IEEE/CVF Conference on Computer Vision and Pattern Recognition* 586–595 (2018).
124. Lehtinen, J. et al. Noise2Noise: learning image restoration without clean data. In *35th International Conference on Machine Learning, ICML 2018* 4620–4631 (2018).
125. Kefer, P. et al. Performance of deep learning restoration methods for the extraction of particle dynamics in noisy microscopy image sequences. *Mol. Biol. Cell* **32**, 903–914 (2021).
126. Wu, Y. et al. Reflective imaging improves spatiotemporal resolution and collection efficiency in light sheet microscopy. *Nat. Commun.* **8**, 1452 (2017).
127. Shaevitz, J. W. & Fletcher, D. A. Enhanced three-dimensional deconvolution microscopy using a measured depth-varying point-spread function. *J. Opt. Soc. Am. A* **24**, 2622–2627 (2007).
128. Yanny, K., Monakhova, K., Shuai, R. W. & Waller, L. Deep learning for fast spatially varying deconvolution. *Optica* **9**, 96–99 (2022).
129. Guo, M. et al. Rapid image deconvolution and multiview fusion for optical microscopy. *Nat. Biotechnol.* **38**, 1337–1346 (2020).

Acknowledgements

We thank Grant Kroeschell and Richard Ikegami (Shroff lab) as well as Jiji Chen (NIH Advanced Imaging and Microscopy Resource) for help with figure preparation. This work was supported by the Howard Hughes Medical Institute (HHMI) and the École Polytechnique Fédérale de Lausanne (EPFL).

Author contributions

The authors contributed equally to all aspects of the article.

Competing interests

H.S. is co-inventor on US patent 9,696,534, owned by NIH and licensed to VisiTech International and Yokogawa Electric Corporation, describing multi-focal and analogue implementations of structured illumination microscopy (SIM), including the instant SIM mentioned here. H.S. has also filed invention disclosures on four-beam SIM and multi-view confocal microscopy, both of which rely on the deep learning strategies mentioned here.

Review article

Additional information

Peer review information *Nature Reviews Molecular Cell Biology* thanks Ricardo Henriques, who co-reviewed with Estibaliz Gómez de Mariscal, Lothar Schermelleh and the other, anonymous, reviewer(s) for their contribution to the peer review of this work.

Publisher's note Springer Nature remains neutral with regard to jurisdictional claims in published maps and institutional affiliations.

Springer Nature or its licensor (e.g. a society or other partner) holds exclusive rights to this article under a publishing agreement with the author(s) or other rightsholder(s); author self-archiving of the accepted manuscript version of this article is solely governed by the terms of such publishing agreement and applicable law.

Related links

CSBDeep: <https://csbdeep.bioimagecomputing.com>
Figshare for ref.¹⁰³: <https://doi.org/10.6084/m9.figshare.c.4537607>
FIJI n2v: <https://imagej.net/plugins/n2v>
FIJI nlm: <https://imagej.net/plugins/non-local-means-denoise/>
GitHub 3D-RCAN: <https://github.com/AiviaCommunity/3D-RCAN>
GitHub autopilot: <https://microscopeautopilot.github.io/>
GitHub CSBDeep: <https://github.com/CSBDeep/CSBDeep>
GitHub DL-SR: <https://github.com/qc17-THU/DL-SR>

GitHub etSTED: <https://github.com/jonatanalvelid/etSTED-widget-base>

GitHub JiLabAO: <https://github.com/JiLabUCBerkeley/JiLabAO>

GitHub Knerlab: <https://github.com/Knerlab>

GitHub n2v: <https://github.com/juglab/n2v>

GitHub phasenet: <https://github.com/mpicbg-csbd/phasenet>

GitHub prevedel-lab/AO: <https://github.com/prevedel-lab/AO.git>

GitHub PSSR: <https://github.com/BPHO-Salk/PSSR>

GitHub pycudasirecon: <https://github.com/tlambert03/pycudasirecon>

GitHub rDL-SIM: <https://github.com/qc17-THU/rDL-SIM>

GitHub Richardson-Lucy-Net: <https://github.com/MeatyPlus/Richardson-Lucy-Net>

GitHub SIMreconProject: <https://github.com/eexuesong/SIMreconProject>

GitHub Sparse-SIM: <https://github.com/WeisongZhao/Sparse-SIM>

GitHub Testa Lab: <https://github.com/TestaLab>

GitHub UNMIX-ME: <https://github.com/jasontsmith2718/UNMIX-ME>

Google Code msim: <http://code.google.com/p/msim/>

Micro-manager EDA plugin: <https://pypi.org/project/eda-plugin/>

Napari n2v: <https://www.piwheels.org/project/napari-n2v/>

Napari nlm: <https://www.napari-hub.org/plugins/napari-nlm>

Skimage nlm: https://scikit-image.org/docs/stable/auto_examples/filters/plot_nonlocal_means.html

Zenodo Henry Pinkard (2020): <https://doi.org/10.5281/zenodo.4314107>

© Springer Nature Limited 2024